EXPERIMENT AND NUMERICAL MODELING FOR REVETMENT AND SILL IN REDUCING SHORE EROSION AND WAVE OVERTOPPING

BY

Z. TUGCE YUKSEL AND NOBUHISA KOBAYASHI

RESEARCH REPORT NO. CACR-19-04

May 2019

CENTER FOR APPLIED COASTAL RESEARCH

Ocean Engineering Laboratory
University of Delaware
Newark, Delaware 19716

ACKNOWLEDGMENTS

I would like to thank our Scientific and Technological Research Council of Turkey (TUBITAK) by supporting this research during my 1-year stay at the Center for Applied Coastal Research, University of Delaware, Newark, Delaware. This study was also supported partly by the U.S. Army Corps of Engineers, Engineer Research and Development Center under Agreement No. W912HZ18P0134.

TABLE OF CONTENTS

LIST OF TABLES

LIST OF FIGURES

ABSTRACT

A laboratory experiment was conducted in a wave flume to compare sand beach profile evolution and wave overtopping of a sand berm for the 3 cases of (i) no structure, (ii) a stone revetment protecting the steep sand berm, and (iii) a stone sill reducing wave action on the berm. The revetment reduced onshore sand transport on the fronting beach but was effective in protecting the sand berm and reducing wave overtopping. The revetment crest was damaged during major wave overtopping. The sill reduced the beach profile change but was not very effective in reducing wave overtopping and berm erosion when the sill crest was submerged sufficiently. An existing numerical model (CSHORE) was upgraded for its application to the sill test where the emerged sill crest became submerged during the test. The upgraded model was compared with the measured wave transformation, wave overtopping and overwash rates, and beach profile evolution in the 3 tests consisting of 90 runs with each run lasting 400 s. The model was also used to predict the settlement of the revetment and sill for the case of no filter below the stone structure. The limited experiment and numerical modelling quantified the capability and limitation of the revetment and sill.

Chapter 1

INTRODUCTION

Stone revetments are conventionally used to protect eroding shores and reduce wave overtopping and damage to backshore areas. Revetments constructed on estuarine shorelines may eliminate buffering wetlands and tidal habitat [e.g., Needelman et al. (2012)]. Sills (low-crested rubble mounds) are constructed to protect planted marshes in living shoreline projects [e.g., Hardaway et al. (2010)]. No established method exists to design the sill geometry and its distance from the eroding shore partly because of the difficulty in quantifying the resistance strength of marshes. Sills also provide partial shore protection before marsh planting. The revetment and sill were discussed for living shoreline projects but have not been compared in quantitative manners. This study compares the two different stone structures in terms of their efficacies in reducing shore erosion and wave overtopping.

Engineering manuals are available for the design of stone structures against wind waves [e.g., USACE (2002)]. These manuals are essentially limited to structures on fixed bottoms below the still water level. An estuarine revetment is normally constructed above the mean high-water level to reduce its effect on the adjacent marsh or beach. A sill is somewhat similar to a submerged breakwater installed at the toe of a perched nourished beach [e.g., Musumeci et al. (2012); Faraci et al. (2014)] but the sill crest is typically above the mean low water level. The sill for living shoreline projects is related to the reef breakwater proposed by Ahrens (1989) for beach stabilization and shore protection. The reef breakwater is designed to allow wave overtopping and transmission as well as some stone movement and structure stabilization. Examples of the sill and revetment are given in Figures 1 and 2.

Figure 1: Typical sill (Living shoreline engineering guidelines New Jersey Department of Environmental Protection, 2016)

Figure 2: Revetment (Ventura Rock Revetment, Ventura River Ecosystem, 2017)

A laboratory experiment consisting of 3 tests was conducted in a wave flume to examine irregular wave transformation on a sand beach without and with a stone structure in the surf and swash zone. For simplicity, no marsh was included and fine sand was used in the experiment. The first test was conducted to quantify shore erosion and wave overtopping for the case of no structure. The second and third tests were for the rebuilt shore protected by a stone revetment and a stone sill, respectively. The stones used in the revetment and sill were identical. The hydrodynamic and morphological data for the 3 tests are compared to quantify the efficacies of the revetment and sill in reducing shore erosion and wave overtopping. The data were also used to extend the cross-shore numerical model CSHORE (Kobayashi 2016) for the prediction of sand transport in the vicinity of the porous revetment and sill. The experiment, data analysis, numerical model extension, and comparison with the data are presented in the following.

Chapter 2

EXPERIMENT

An experiment was conducted in a wave flume that is 23 m long, 1.15 m wide, and 1.5 m high as shown in Figure 3. The sand beach in the flume consisted of well-sorted fine sand with a median diameter of 0.18 mm. The fine sand was observed to be transported as both bed load and suspended load. The measured fall velocity, density, and porosity of the sand were 2.0 cm/s, 2.6 g/cm^3, and 0.4, respectively. A 400-s run of irregular waves with a Texel, Marsen, and Arsloe (TMA) spectrum was generated by the piston-type wavemaker in a water depth of 88, 92, and 96cm. The still water level (SWL) was raised by an increment of 4 cm. The spectral significant wave height and peak period were approximately 19 cm and 2.6 s. Eight wave gauges (WG1 – WG8) were used to measure the free surface elevation from the wave shoaling zone to the swash zone. WG9 was used to measure the water level in the basin after each run to collect the volume of overtopped water. The wave overtopping rate q_o and sand overwash rate q_{bs} were measured by collecting overtopped water and sand in the water collection basin and sand trap during each 400-s run. The fluid velocities in the surf zone were measured by three velocimeters: one two-dimensional (2D) acoustic Doppler velocimeter (ADV) and two Vectrinos (Nortek, Rud, Norway) at an elevation above the bed of one-third of the local water depth. A vertical wall was located at the onshore coordinate x = 19.9 m with $x = 0$ at WG1. The vertical coordinate z was positive upward with $z = 0$ at the still-water level of 88-cm water depth. The elevation of the wall crest was 1.07 m above the horizontal flume bottom. The wave overtopping rate and sand overwash rate were measured by collecting overtopped water and sand in a water collection basin and a sand trap during each 400-s run. The beach profile was measured using a laser line scanner system (Figlus

et al. 2011) every 10 runs. Three-dimensional bathymetry data were averaged alongshore after confirmation of alongshore uniformity. The initial profile at the beginning of the experiment is depicted in Figure 3.

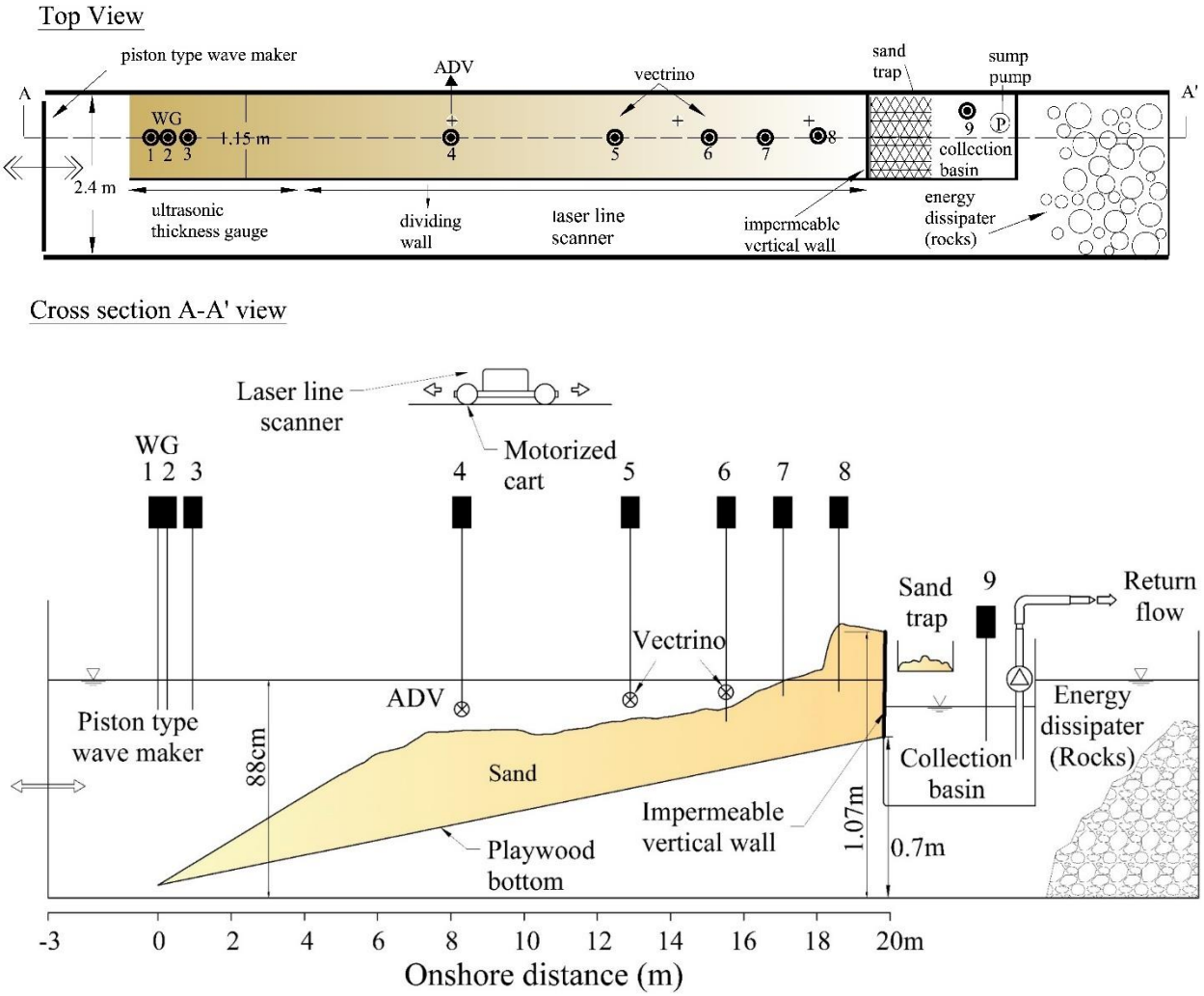

Figure 3: Experimental setup at start of Test N with no structure

Table 1 lists three tests conducted in sequence. Figure 4 shows the initial profile with the SWLs at elevation z = 0, 4, and 8 cm for each test. The initial profile of the no (N) protection test was created from the equilibrium beach profile which existed in the flume after the previous

experiment by Kobayashi et al. (2018). The foreshore slope of approximately 1/8 (vertical/horizontal) was steepened to about 1/3 by moving the foreshore sand to the berm crest and to the beach at the toe of the steepened slope in order to induce shore erosion. The fronting beach slope was about 1/24. The initial beach profile may have been artificial but the N test provides an insight into the effect of grading on cross-shore sand transport. The initial profile was exposed to 10 runs with each run lasting 400-s and the beach profile was measured. The SWL was raised by 4 cm and the profile was measured again after another 10 runs. The SWL was increased to 8 cm so as to cause significant erosion and wave overtopping. The final profile was measured again after another 10 runs.

Table 1: Sequence of Three Tests with Three Still Water Levels

Test	Description	SWL (cm)	No. of Runs	Time (s)
N	No Protection	0	10	0 – 4,000
		4	10	4,000 – 8,000
		8	10	8,000 – 12,000
R	Revetment	0	10	0 – 4,000
		4	10	4,000 – 8,000
		8	10	8,000 – 12,000
S	Sill	0	10	0 – 4,000
		4	10	4,000 – 8,000
		8	10	8,000 – 12,000

The initial steep slope profile was rebuilt and a stone revetment was placed on a filter of polyester fabric mesh with an opening of 0.074 mm for the revetment (R) test in Figure 4. The mesh edges were buried 0.1 m into the sand to minimize sand undermining below the fabric mesh because the stone seawall experiment by Kobayashi and Kim (2017) indicated significant sand undermining below the same fabric mesh with open mesh edges. The revetment was constructed of the green and blue stones used by Kobayashi and Kim (2017). The nominal diameters of the green and blue stones were 3.52 and 3.81 cm, respectively. The porosity was 0.44 for both stones. The green and blue stone segment widths across the 115-cm wide flume were 62 and 53 cm, respectively (Kim et al., 2016). The stones were placed randomly in a two-layer thickness in the zone of x = 18.12 – 18.52 m. The revetment slope varied but was about 1/2. The initial profiles before and after the stone placement were measured and the testing procedure for the N test was repeated. The stones were removed at the end of the R test to measure the deposited sand height above the filter and the filter elevation using the procedure adopted by Garcia and Kobayashi (2015).

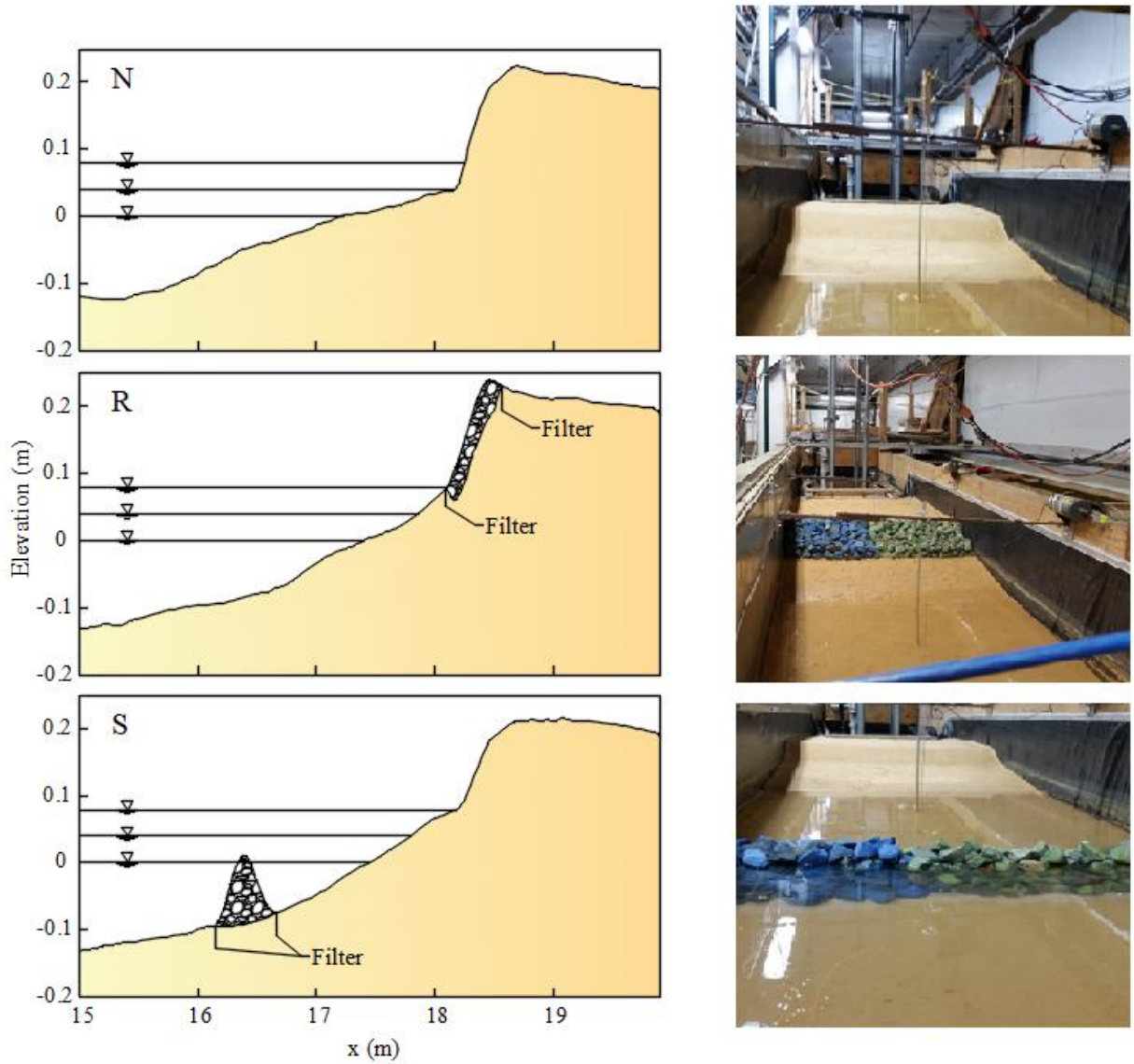

Figure 4: Initial profiles of Tests N, R, and S with SWL of 0, 4, and 8 cm (photos represent tests N, R, and S with SWL of 0 cm)

The testing procedure for the sill (S) test was the same as that for the revetment test except for the location and geometry of the sill structure. The same stones were used for both structures because the structure cost depends on the amount and characteristic of stones. The sill location in the zone of x = 16.16 – 16.64 m was chosen so that the initial sill crest was emerged, near the

SWL, and submerged for the SWL of 0, 4, and 8 cm, respectively. The side slopes of the sill were approximately 1/2. The crest width was about 6 cm and less than a traditional three-stone width [e.g., Melby and Kobayashi (1998)]. The sill stones were piled loosely to allow some stone movement and stabilization. The fabric mesh edges were extended less than 0.1 m on the sand surface and then buried 0.1 m in the sand. The mesh edge extension was intended to support displaced stones on the filter. The extended filter was covered with a thin layer of sand. It is noted that the careful preparation of the sill filter was prompted by the filter settlement measured after the R test in spite of the 0.1 m burial of the mesh edge.

Chapter 3

DATA ANALYSIS

3.1 Free Surface and Velocity Statistics

The time series for Wave Gauges WG1 – WG3, located at x = 0.0, 0.25, and 0.95 m, respectively, were used to separate incident and reflected waves at the location of x = 0 for each run. The separation method was explained by Kobayashi et al. (1990). The spectral significant wave height H_{mo} and peak period T_p of the incident waves were approximately 19 cm and 2.6 s. The reflection coefficient, defined as the ratio between the values of H_{mo} for the reflected and incident waves was less than 0.2 because the steep slope toe in Figure 4 were located above or near the SWLs of 0, 4, and 8 cm. The reflection coefficient increased about 0.03 with the increase of the SWL.

The measured time series of the free surface elevation η above the SWL and the velocities for each of the 90 runs in the N, R, and S tests were analyzed to examine the cross- shore wave transformation. The measured alongshore and vertical velocities were small in comparison to the cross-shore velocity u. The mean and standard deviation of η and u were calculated to compare the wave transformation in the three tests. The averaging of WG8 located above the berm in Figure 3 and buried partially in the sand was performed for the wet duration. The wet probability P_w was defined as the ratio of the wet duration and the total duration. These measured values for 10 runs with the given SWL were averaged and the averaged values for the N, R, and S tests were compared to examine the effects of the revetment and sill on the wave transformation.

Tables 2 – 10 list the incident wave characteristics at the location x=0 of WG1 for the N, R, and S test series. In these tables, H_{rms} = root-mean-square wave height, H_s = significant wave height, T_s= significant wave period, and R = wave reflection coefficient (Kobayashi et al. 1990). Tables 11 – 46 include the analyzed results for the mean and standard deviation of η and u, and the wet probability P_w, bottom elevation z_b, and mean depth $\overline{h}$ at WG8.

For convenience, use is made of time t = 0 – 4,000 s with SWL = 0 cm for Low (L) water level, t = 4,000 – 8,000 s with SWL = 4 cm for Medium (M) water level, t = 8,000 – 12,000 s with SWL = 8 cm for High (H) water level in Tables 2 – 52. The letters of L, M, and H are attached before the test names of N, R, and S. The run number (1 to 10) indicates the temporal sequence of runs (400 s for each run) starting from run 1 for each SWL denoted by the two letters (SWL and test).

Table 2: Incident wave characteristics for N test series, SWL = 0 cm

Run	H_{mo} (cm)	H_{rms} (cm)	H_s (cm)	T_p (s)	T_s (s)	R
LN1	18.64	13.18	18.12	2.62	2.14	0.14
LN2	19.09	13.50	18.28	2.62	2.14	0.14
LN3	19.23	13.60	18.50	2.62	2.14	0.14
LN4	19.23	13.60	18.54	2.62	2.14	0.14
LN5	19.22	13.60	18.61	2.62	2.12	0.14
LN6	19.18	13.56	18.48	2.62	2.12	0.14
LN7	19.14	13.53	18.40	2.62	2.13	0.14
LN8	19.11	13.51	18.40	2.62	2.13	0.14
LN9	19.03	13.46	18.32	2.62	2.12	0.14
LN10	19.02	13.45	18.20	2.62	2.13	0.14
Average	**19.10**	**13.50**	**18.36**	**2.62**	**2.13**	**0.14**

Table 3: Incident wave characteristics for N test series, SWL = 4 cm

Run	H_{mo} (cm)	H_{rms} (cm)	H_s (cm)	T_p (s)	T_s (s)	R
MN1	18.40	13.01	17.62	2.62	2.18	0.19
MN2	19.36	13.70	18.68	2.62	2.14	0.17
MN3	19.73	13.95	19.17	2.62	2.16	0.16
MN4	19.93	14.09	19.40	2.62	2.16	0.16
MN5	20.08	14.20	19.50	2.62	2.16	0.16
MN6	20.01	14.15	19.40	2.62	2.16	0.16
MN7	19.97	14.12	19.47	2.62	2.16	0.16
MN8	19.92	13.91	19.28	2.62	2.15	0.16
MN9	19.94	14.10	19.32	2.62	2.16	0.16
MN10	19.89	14.06	19.50	2.62	2.17	0.16
Average	**19.72**	**13.93**	**19.13**	**2.62**	**2.16**	**0.16**

Table 4: Incident wave characteristics for N test series, SWL = 8 cm

Run	H_{mo} (cm)	H_{rms} (cm)	H_s (cm)	T_p (s)	T_s (s)	R
HN1	18.79	13.28	18.40	2.62	2.15	0.20
HN2	19.13	13.52	18.68	2.62	2.14	0.19
HN3	17.53	12.40	16.98	2.62	2.16	0.18
HN4	17.88	12.64	17.27	2.62	2.15	0.18
HN5	18.08	12.80	17.62	2.62	2.13	0.16
HN6	17.66	12.48	17.06	2.62	2.11	0.16
HN7	17.91	12.67	17.30	2.62	2.10	0.17
HN8	18.07	12.78	17.43	2.62	2.13	0.17
HN9	18.15	12.83	17.60	2.62	2.14	0.17
HN10	18.18	12.86	17.60	2.62	2.12	0.16
Average	**18.14**	**12.83**	**17.60**	**2.62**	**2.13**	**0.17**

Table 5: Incident wave characteristics for R test series, SWL = 0 cm

Run	H_{mo} (cm)	H_{rms} (cm)	H_s (cm)	T_p (s)	T_s (s)	R
LR1	17.22	12.47	16.70	2.62	2.16	0.15
LR2	17.75	12.85	16.02	2.62	2.13	0.15
LR3	17.90	12.95	16.41	2.62	2.17	0.15
LR4	17.42	12.61	16.84	2.62	2.17	0.15
LR5	17.88	12.94	16.31	2.62	2.13	0.15
LR6	17.09	12.09	16.38	2.62	2.14	0.15
LR7	17.07	12.07	16.45	2.62	2.15	0.17
LR8	17.05	12.06	16.39	2.62	2.14	0.15
LR9	16.97	12.00	16.13	2.62	2.12	0.16
LR10	17.05	12.06	16.40	2.62	2.14	0.16
Average	**17.34**	**12.41**	**16.40**	**2.62**	**2.15**	**0.15**

Table 6: Incident wave characteristics for R test series, SWL = 4 cm

Run	H_{mo} (cm)	H_{rms} (cm)	H_s (cm)	T_p (s)	T_s (s)	R
MR1	18.95	13.40	18.17	2.62	2.15	0.19
MR2	19.34	13.67	18.48	2.62	2.13	0.20
MR3	19.53	13.81	18.70	2.62	2.16	0.22
MR4	19.53	13.81	18.68	2.62	2.14	0.22
MR5	19.60	13.86	18.83	2.62	2.13	0.22
MR6	19.56	13.83	18.77	2.62	2.14	0.23
MR7	19.60	13.86	18.77	2.62	2.17	0.22
MR8	19.47	13.77	18.77	2.62	2.15	0.21
MR9	19.47	13.77	18.68	2.62	2.14	0.21
MR10	19.44	13.75	18.74	2.62	2.14	0.21
Average	**19.44**	**13.75**	**18.65**	**2.62**	**2.15**	**0.21**

Table 7: Incident wave characteristics for R test series, SWL = 8 cm

Run	H_{mo} (cm)	H_{rms} (cm)	H_s (cm)	T_p (s)	T_s (s)	R
HR1	18.32	12.96	17.47	2.62	2.14	0.20
HR2	18.53	13.10	17.54	2.62	2.14	0.20
HR3	18.77	13.27	17.87	2.62	2.14	0.20
HR4	19.11	13.51	18.19	2.62	2.13	0.21
HR5	19.32	13.66	18.71	2.62	2.12	0.21
HR6	19.31	13.66	18.61	2.62	2.13	0.21
HR7	19.39	13.71	18.68	2.62	2.14	0.22
HR8	19.56	13.83	18.77	2.62	2.12	0.21
HR9	19.31	13.65	18.72	2.62	2.13	0.21
HR10	19.36	13.69	18.70	2.62	2.14	0.21
Average	**19.10**	**13.50**	**18.32**	**2.62**	**2.13**	**0.21**

Table 8: Incident wave characteristics for S test series, SWL = 0 cm

Run	H_{mo} (cm)	H_{rms} (cm)	H_s (cm)	T_p (s)	T_s (s)	R
LS1	18.30	12.94	17.63	2.62	2.16	0.16
LS2	18.69	13.22	18.03	2.62	2.16	0.15
LS3	18.95	13.40	18.22	2.62	2.13	0.15
LS4	19.13	13.52	18.54	2.62	2.15	0.16
LS5	19.12	13.52	18.34	2.62	2.13	0.16
LS6	19.10	13.51	18.32	2.62	2.14	0.15
LS7	19.09	13.50	18.34	2.62	2.13	0.16
LS8	19.09	13.50	18.37	2.62	2.14	0.15
LS9	19.06	13.48	18.30	2.62	2.15	0.16
LS10	19.05	13.46	18.38	2.62	2.14	0.16
Average	**18.96**	**13.41**	**18.25**	**2.62**	**2.14**	**0.16**

Table 9: Incident wave characteristics for S test series, SWL = 4 cm

Run	H_{mo} (cm)	H_{rms} (cm)	H_s (cm)	T_p (s)	T_s (s)	R
MS1	18.49	13.08	17.75	2.62	2.19	0.22
MS2	18.83	13.32	18.18	2.62	2.12	0.17
MS3	19.02	13.45	18.40	2.62	2.14	0.19
MS4	19.26	13.62	18.84	2.62	2.14	0.18
MS5	20.03	14.16	19.33	2.62	2.18	0.16
MS6	20.09	14.20	19.37	2.62	2.17	0.16
MS7	20.02	14.15	19.44	2.62	2.19	0.16
MS8	20.02	14.15	19.34	2.62	2.16	0.16
MS9	20.02	14.15	19.30	2.62	2.16	0.16
MS10	19.05	13.46	18.38	2.62	2.14	0.16
Average	**19.48**	**13.77**	**18.83**	**2.62**	**2.16**	**0.17**

Table 10: Incident wave characteristics for S test series, SWL = 8 cm

Run	H_{mo} (cm)	H_{rms} (cm)	H_s (cm)	T_p (s)	T_s (s)	R
HS1	19.74	13.96	19.45	2.62	2.19	0.18
HS2	19.06	13.48	18.80	2.62	2.20	0.17
HS3	19.85	14.74	19.50	2.62	2.17	0.17
HS4	19.19	14.28	18.84	2.62	2.18	0.17
HS5	19.94	14.80	19.47	2.62	2.14	0.16
HS6	20.04	14.88	19.45	2.62	2.14	0.16
HS7	20.04	14.88	19.60	2.62	2.17	0.16
HS8	20.07	14.90	19.56	2.62	2.16	0.16
HS9	20.05	14.88	19.52	2.62	2.14	0.16
HS10	20.01	14.86	19.54	2.62	2.15	0.16
Average	**19.79**	**14.56**	**19.37**	**2.62**	**2.16**	**0.17**

Table 11: Mean free-surface elevation $\overline{\eta}$ (cm) at seven wave gauge locations for N test series, SWL = 0 cm

Run	WG1	WG2	WG3	WG4	WG5	WG6	WG7
LN1	-0.24	-0.24	-0.17	-0.09	0.30	0.28	1.31
LN2	-0.19	-0.22	-0.18	-0.07	0.32	0.12	0.40
LN3	-0.19	-0.18	-0.21	-0.08	0.34	-1.66	0.38
LN4	-0.19	-0.21	-0.20	-0.08	0.34	1.73	1.02
LN5	-0.19	-0.20	-0.21	-0.07	0.34	1.74	0.82
LN6	-0.16	-0.18	-0.19	-0.05	0.34	1.16	0.72
LN7	-0.18	-0.19	-0.21	-0.05	0.34	NR	0.52
LN8	-0.17	-0.20	-0.18	-0.05	0.33	NR	0.66
LN9	-0.17	-0.17	-0.17	-0.06	0.32	NR	0.70
LN10	-0.15	-0.17	-0.17	-0.03	0.33	1.23	0.43
Average	**-0.18**	**-0.19**	**-0.19**	**-0.06**	**0.33**	**0.65**	**0.69**

Table 12: Mean free-surface elevation $\overline{\eta}$ (cm) at seven wave gauge locations for N test series, SWL = 4 cm

Run	WG1	WG2	WG3	WG4	WG5	WG6	WG7
MN1	-0.20	-0.21	-0.21	-0.15	0.10	0.11	0.10
MN2	-0.20	-0.20	-0.15	-0.13	0.10	0.12	0.20
MN3	-0.12	-0.14	-0.15	-0.10	0.14	0.14	0.17
MN4	-0.11	-0.15	-0.15	-0.10	0.15	0.17	0.15
MN5	-0.11	-0.15	-0.14	-0.11	0.15	0.18	0.15
MN6	-0.10	-0.14	-0.16	-0.09	0.15	0.20	0.17
MN7	-0.14	-0.19	-0.15	-0.10	0.13	0.16	0.22
MN8	-0.13	-0.17	-0.17	-0.09	0.14	0.21	0.23
MN9	-0.11	-0.15	-0.18	-0.07	0.14	0.17	0.27
MN10	-0.15	-0.17	-0.21	-0.11	0.11	0.19	0.24
Average	**-0.14**	**-0.17**	**-0.17**	**-0.10**	**0.13**	**0.16**	**0.19**

Table 13: Mean free-surface elevation $\overline{\eta}$ (cm) at seven wave gauge locations for N test series, SWL = 8 cm

Run	WG1	WG2	WG3	WG4	WG5	WG6	WG7
HN1	-0.28	-0.28	-0.34	-0.26	0.10	0.11	0.17
HN2	-0.22	-0.22	-0.29	-0.22	-0.09	0.40	0.11
HN3	-0.17	-0.18	-0.29	-0.27	0.14	0.13	0.22
HN4	-0.15	-0.18	-0.15	-0.30	0.08	0.11	0.14
HN5	-0.17	-0.21	-0.30	-0.24	0.06	0.10	0.12
HN6	-0.17	-0.19	-0.26	-0.24	-0.07	0.04	0.15
HN7	-0.14	-0.17	-0.28	-0.22	-0.06	0.08	0.10
HN8	-0.13	-0.18	-0.27	-0.23	-0.04	0.08	0.11
HN9	-0.13	-0.16	-0.25	-0.22	-0.02	0.06	0.09
HN10	-0.14	-0.16	-0.24	-0.23	-0.04	0.08	0.16
Average	**-0.17**	**-0.19**	**-0.26**	**-0.24**	**0.006**	**0.12**	**0.14**

Table 14: Mean free-surface elevation $\overline{\eta}$ (cm) at seven wave gauge locations for R test series, SWL = 0 cm

Run	WG1	WG2	WG3	WG4	WG5	WG6	WG7
LR1	-0.08	-0.10	-0.17	-0.09	0.23	0.38	0.42
LR2	-0.14	-0.17	-0.19	-0.11	0.29	0.39	0.45
LR3	-0.12	-0.16	-0.19	-0.05	0.29	0.43	0.48
LR4	-0.14	-0.14	-0.18	-0.07	0.27	0.42	0.48
LR5	-0.15	-0.20	-0.20	-0.04	0.27	0.41	0.47
LR6	-0.13	-0.18	-0.18	-0.02	0.32	0.45	0.53
LR7	-0.13	-0.19	-0.20	-0.01	0.31	0.47	0.54
LR8	-0.11	-0.17	-0.19	-0.05	0.32	0.45	0.56
LR9	-0.14	-0.19	-0.18	-0.03	0.34	0.47	0.49
LR10	-0.14	-0.17	-0.20	-0.01	0.34	0.45	0.56
Average	**-0.13**	**-0.17**	**-0.18**	**-0.05**	**0.29**	**0.43**	**0.49**

Table 15: Mean free-surface elevation $\overline{\eta}$ (cm) at seven wave gauge locations for R test series, SWL = 4 cm

Run	WG1	WG2	WG3	WG4	WG5	WG6	WG7
MR1	-0.21	-0.19	-0.25	-0.17	0.17	0.27	0.22
MR2	-0.15	-0.16	-0.26	-0.10	0.24	0.39	0.33
MR3	-0.13	-0.17	-0.26	-0.09	0.26	0.34	0.31
MR4	-0.17	-0.18	-0.29	-0.11	0.23	0.31	0.29
MR5	-0.15	-0.17	-0.26	-0.10	0.27	0.32	0.34
MR6	-0.15	-0.18	-0.28	-0.09	0.27	0.34	0.34
MR7	-0.17	-0.17	-0.29	-0.09	0.25	0.29	0.34
MR8	-0.15	-0.16	-0.28	-0.07	0.25	0.34	0.36
MR9	-0.16	-0.18	-0.26	-0.10	0.21	0.29	0.35
MR10	-0.16	-0.17	-0.26	-0.06	0.26	0.34	0.38
Average	**-0.16**	**-0.17**	**-0.27**	**-0.09**	**0.24**	**0.32**	**0.32**

Table 16: Mean free-surface elevation $\overline{\eta}$ (cm) at seven wave gauge locations for R test series, SWL = 8 cm

Run	WG1	WG2	WG3	WG4	WG5	WG6	WG7
HR1	-0.12	-0.12	-0.21	-0.18	-0.03	0.15	0.07
HR2	-0.13	-0.16	-0.24	-0.16	0.03	0.13	0.15
HR3	-0.12	-0.14	-0.22	-0.18	0.07	0.16	0.15
HR4	-0.13	-0.14	-0.23	-0.15	0.06	0.18	0.14
HR5	-0.14	-0.15	-0.22	-0.16	0.04	0.16	0.15
HR6	-0.13	-0.15	-0.23	-0.17	0.03	0.14	0.14
HR7	-0.12	-0.16	-0.25	-0.16	0.05	0.16	0.17
HR8	-0.15	-0.16	-0.25	-0.19	0.02	0.15	0.16
HR9	-0.14	-0.17	-0.24	-0.17	0.03	0.17	0.25
HR10	-0.15	-0.16	-0.23	-0.15	0.08	0.18	0.23
Average	**-0.13**	**-0.15**	**-0.23**	**-0.16**	**0.04**	**0.15**	**0.16**

Table 17: Mean free-surface elevation $\overline{\eta}$ (cm) at seven wave gauge locations for S test series, SWL = 0 cm

Run	WG1	WG2	WG3	WG4	WG5	WG6	WG7
LS1	-0.24	-0.24	-0.18	0.05	0.36	0.55	0.56
LS2	-0.22	-0.26	-0.19	0.06	0.44	0.57	0.59
LS3	-0.19	-0.25	-0.20	0.10	0.44	0.58	0.67
LS4	-0.19	-0.24	-0.20	0.07	0.45	0.58	0.61
LS5	-0.19	-0.25	-0.21	0.08	0.44	0.56	0.62
LS6	-0.18	-0.25	-0.20	0.08	0.46	0.61	0.74
LS7	-0.21	-0.24	-0.20	0.09	0.44	0.60	0.72
LS8	-0.20	-0.25	-0.20	0.09	0.45	0.60	0.76
LS9	-0.20	-0.25	-0.21	0.08	0.45	0.58	0.69
LS10	-0.21	-0.27	-0.19	0.08	0.43	0.60	0.71
Average	**-0.20**	**-0.25**	**-0.19**	**0.08**	**0.44**	**0.58**	**0.66**

Table 18: Mean free-surface elevation $\overline{\eta}$ (cm) at seven wave gauge locations for S test series, SWL = 4 cm

Run	WG1	WG2	WG3	WG4	WG5	WG6	WG7
MS1	-0.19	-0.19	-0.26	-0.01	0.22	0.27	0.38
MS2	-0.18	-0.18	-0.28	0.00	0.24	0.29	0.31
MS3	-0.18	-0.20	-0.30	0.01	0.27	0.32	0.33
MS4	-0.17	-0.20	-0.28	0.01	0.28	0.32	0.39
MS5	-0.16	-0.19	-0.21	0.01	0.25	0.33	0.35
MS6	-0.12	-0.19	-0.19	0.01	0.27	0.38	0.42
MS7	-0.13	-0.19	-0.19	0.03	0.26	0.36	0.47
MS8	-0.16	-0.18	-0.22	0.04	0.25	0.36	0.42
MS9	-0.15	-0.18	-0.19	0.03	0.27	0.36	0.41
MS10	-0.17	-0.18	-0.20	0.02	0.29	0.36	0.44
Average	**-0.16**	**-0.18**	**-0.23**	**0.02**	**0.26**	**0.34**	**0.39**

Table 19: Mean free-surface elevation $\overline{\eta}$ (cm) at seven wave gauge locations for S test series, SWL = 8 cm

Run	WG1	WG2	WG3	WG4	WG5	WG6	WG7
HS1	-0.23	-0.28	-0.22	-0.21	-0.07	-0.07	0.40
HS2	-0.16	-0.21	-0.21	-0.21	-0.10	0.00	0.33
HS3	-0.15	-0.19	-0.20	-0.16	0.05	0.15	0.50
HS4	-0.11	-0.12	-0.23	-0.14	-0.02	0.12	0.47
HS5	-0.18	-0.20	-0.20	-0.17	0.01	0.11	0.49
HS6	-0.15	-0.19	-0.18	-0.12	0.06	0.17	0.56
HS7	-0.15	-0.18	-0.18	-0.13	0.06	0.21	0.55
HS8	-0.18	-0.20	-0.20	-0.17	0.01	0.14	0.49
HS9	-0.15	-0.19	-0.18	-0.14	0.05	0.16	0.52
HS10	-0.16	-0.20	-0.19	-0.13	0.06	0.19	0.53
Average	**-0.16**	**-0.19**	**-0.19**	**-0.16**	**0.01**	**0.12**	**0.48**

Table 20: Free-surface standard deviation σ_η (cm) at seven wave gauge locations for N test series, SWL = 0 cm

Run	WG1	WG2	WG3	WG4	WG5	WG6	WG7
LN1	4.44	4.52	4.42	3.67	2.65	2.26	1.65
LN2	4.55	4.61	4.51	3.73	2.66	2.36	1.67
LN3	4.59	4.65	4.55	3.70	2.68	3.18	1.71
LN4	4.58	4.64	4.55	3.73	2.68	2.84	1.76
LN5	4.58	4.64	4.54	3.72	2.70	2.90	1.81
LN6	4.57	4.64	4.54	3.72	2.70	2.51	0.72
LN7	4.56	4.62	4.52	3.70	2.70	2.72	0.52
LN8	4.56	4.62	4.51	3.70	2.71	2.14	1.86
LN9	4.53	4.61	4.50	3.71	2.70	2.91	1.89
LN10	4.54	4.62	4.50	3.70	2.72	2.57	1.90
Average	**4.55**	**4.62**	**4.51**	**3.71**	**2.69**	**2.64**	**1.56**

Table 21: Free-surface standard deviation σ_η (cm) at seven wave gauge locations for N test series, SWL = 4 cm

Run	WG1	WG2	WG3	WG4	WG5	WG6	WG7
MN1	4.41	4.49	4.55	3.88	3.07	2.84	2.58
MN2	4.71	4.77	4.59	3.87	3.03	2.31	2.53
MN3	4.80	4.86	4.66	3.91	3.05	3.14	2.54
MN4	4.85	4.91	4.72	3.95	3.04	2.38	2.58
MN5	4.88	4.94	4.74	3.94	3.05	2.71	2.59
MN6	4.87	4.93	4.73	3.96	3.07	3.24	2.60
MN7	4.86	4.92	4.72	3.93	3.06	3.32	2.60
MN8	4.86	4.90	4.71	3.92	3.06	4.08	2.59
MN9	4.86	4.91	4.71	3.94	3.06	3.13	2.60
MN10	4.84	4.90	4.69	3.90	3.05	3.23	2.60
Average	**4.79**	**4.85**	**4.68**	**3.92**	**3.05**	**3.04**	**2.58**

Table 22: Free-surface standard deviation σ_η (cm) at seven wave gauge locations for N test series, SWL = 8 cm

Run	WG1	WG2	WG3	WG4	WG5	WG6	WG7
HN1	4.60	4.61	4.51	3.88	3.30	3.55	3.19
HN2	4.68	4.69	4.57	3.90	3.29	3.80	3.13
HN3	4.24	4.27	4.31	3.94	3.31	3.11	3.14
HN4	4.32	4.35	4.43	4.00	3.30	3.11	3.07
HN5	4.35	4.39	4.41	4.02	3.31	3.11	3.02
HN6	4.24	4.28	4.32	3.95	3.24	3.07	2.98
HN7	4.29	4.33	4.42	3.99	3.24	3.08	2.95
HN8	4.33	4.38	4.48	4.00	3.26	3.09	2.94
HN9	4.35	4.38	4.47	4.01	3.25	3.09	2.92
HN10	4.35	4.39	4.47	3.98	3.24	3.07	2.90
Average	**4.35**	**4.41**	**4.44**	**3.96**	**3.27**	**3.20**	**3.02**

Table 23: Free-surface standard deviation σ_η (cm) at seven wave gauge locations for R test series, SWL = 0 cm

Run	WG1	WG2	WG3	WG4	WG5	WG6	WG7
LR1	4.84	4.82	3.95	3.58	2.66	2.32	2.05
LR2	4.99	4.97	4.08	3.65	2.68	2.29	2.06
LR3	4.04	4.01	4.12	3.65	2.69	2.30	2.11
LR4	3.92	3.90	4.04	3.62	2.65	2.28	2.10
LR5	4.02	4.00	4.09	3.63	2.66	2.28	2.12
LR6	4.09	4.07	4.15	3.67	2.70	2.29	2.13
LR7	4.10	4.07	4.21	3.67	2.71	2.31	2.15
LR8	4.10	4.07	4.18	3.66	2.72	2.31	2.16
LR9	4.09	4.09	4.17	3.65	2.71	2.31	2.18
LR10	4.11	4.12	4.15	3.65	2.72	2.32	2.18
Average	**4.33**	**4.31**	**4.11**	**3.64**	**2.69**	**2.30**	**2.12**

Table 24: Free-surface standard deviation σ_η (cm) at seven wave gauge locations for R test series, SWL = 4 cm

Run	WG1	WG2	WG3	WG4	WG5	WG6	WG7
MR1	4.56	4.61	3.61	3.97	3.17	2.86	2.84
MR2	4.68	4.73	4.76	4.03	3.22	2.94	2.84
MR3	4.73	4.77	4.82	4.07	3.25	2.94	2.82
MR4	4.74	4.78	4.84	4.02	3.25	2.96	2.81
MR5	4.75	4.80	4.79	4.03	3.25	2.94	2.81
MR6	4.74	4.79	4.82	4.03	3.25	2.94	2.82
MR7	4.74	4.80	4.81	4.01	3.24	2.94	2.80
MR8	4.73	4.77	4.78	4.00	3.26	2.95	2.79
MR9	4.73	4.77	4.78	4.02	3.25	2.96	2.79
MR10	4.72	4.77	4.77	3.97	3.24	2.94	2.79
Average	**4.71**	**4.75**	**4.67**	**4.02**	**3.24**	**2.94**	**2.81**

Table 25: Free-surface standard deviation σ_η (cm) at seven wave gauge locations for R test series, SWL = 8 cm

Run	WG1	WG2	WG3	WG4	WG5	WG6	WG7
HR1	4.40	4.42	4.92	4.02	3.39	3.13	3.14
HR2	4.49	4.51	5.19	4.06	3.40	3.15	3.17
HR3	4.57	4.57	5.24	4.07	3.42	3.17	3.16
HR4	4.59	4.61	5.27	4.07	3.42	3.17	3.16
HR5	4.58	4.60	4.89	4.09	3.43	3.18	3.14
HR6	4.62	4.60	4.90	4.10	3.43	3.18	3.15
HR7	4.59	4.61	4.94	4.07	3.42	3.18	3.14
HR8	4.62	4.62	5.02	4.07	3.42	3.20	3.20
HR9	4.63	4.64	4.89	4.09	3.43	3.20	3.13
HR10	4.62	4.62	4.86	4.09	3.43	3.20	3.10
Average	**4.57**	**4.58**	**5.01**	**4.07**	**3.42**	**3.17**	**3.15**

Table 26: Free-surface standard deviation σ_η (cm) at seven wave gauge locations for S test series, SWL = 0 cm

Run	WG1	WG2	WG3	WG4	WG5	WG6	WG7
LS1	4.33	4.39	4.41	3.63	2.67	2.32	2.01
LS2	4.43	4.49	4.50	3.63	2.67	2.33	2.11
LS3	4.49	4.55	4.56	3.64	2.69	2.32	2.03
LS4	4.53	4.59	4.60	3.66	2.67	2.35	2.10
LS5	4.52	4.59	4.60	3.66	2.68	2.35	2.12
LS6	4.54	4.59	4.60	3.64	2.69	2.35	2.14
LS7	4.53	4.58	4.60	3.63	2.67	2.35	2.16
LS8	4.53	4.58	4.59	3.62	2.66	2.36	2.21
LS9	4.52	4.58	4.59	3.62	2.67	2.35	2.13
LS10	4.51	4.57	4.58	3.61	2.65	2.33	2.13
Average	**4.49**	**4.55**	**4.56**	**3.63**	**2.67**	**2.34**	**2.12**

Table 27: Free-surface standard deviation σ_η (cm) at seven wave gauge locations for S test series, SWL = 4 cm

Run	WG1	WG2	WG3	WG4	WG5	WG6	WG7
MS1	4.36	4.40	4.68	3.94	3.12	2.75	2.06
MS2	4.59	4.57	4.81	3.95	3.14	2.74	2.05
MS3	4.62	4.64	4.96	3.98	3.12	2.75	2.04
MS4	4.66	4.69	4.84	3.96	3.14	2.76	2.03
MS5	4.70	4.83	4.92	3.95	3.12	2.73	2.13
MS6	4.72	4.85	4.94	3.92	3.13	2.74	2.02
MS7	4.69	4.83	4.91	3.93	3.12	2.75	2.01
MS8	4.70	4.82	4.91	3.89	3.11	2.74	2.00
MS9	4.70	4.83	4.91	3.90	3.12	2.73	2.00
MS10	4.70	4.83	4.91	3.89	3.11	2.74	2.02
Average	**4.64**	**4.73**	**4.87**	**3.93**	**3.12**	**2.74**	**2.04**

Table 28: Free-surface standard deviation σ_η (cm) at seven wave gauge locations for S test series, SWL = 8 cm

Run	WG1	WG2	WG3	WG4	WG5	WG6	WG7
HS1	4.69	4.85	4.80	3.92	3.35	3.01	2.67
HS2	4.53	4.69	4.65	3.84	3.26	2.99	2.64
HS3	4.94	5.09	5.06	4.00	3.38	3.05	2.65
HS4	4.79	4.93	4.89	3.94	3.32	3.02	2.58
HS5	4.96	5.10	5.07	4.00	3.37	3.06	2.57
HS6	4.98	5.12	5.09	4.01	3.36	3.05	2.53
HS7	4.98	5.13	5.09	4.01	3.37	3.04	2.49
HS8	4.99	5.12	5.09	3.99	3.34	3.04	2.47
HS9	4.98	5.12	5.07	3.99	3.34	3.01	2.41
HS10	4.97	5.12	5.07	3.99	3.32	3.02	2.41
Average	**4.88**	**5.02**	**4.98**	**3.96**	**3.34**	**3.03**	**2.54**

Table 29: Wet probability P_w, mean free-surface elevation $\overline{\eta}$ (cm) and free-surface standard deviation σ_η (cm) at WG8 for N test series, SWL = 0 cm

Run	*t (s)*	P_w	z_b *(cm)*	$\overline{h}$ *(cm)*	$\overline{\eta}$ *(cm)*	σ_η *(cm)*
	0		21.50			
LN1	200	0.00	21.51	0.00	21.51	-
LN2	600	0.00	21.52	0.00	21.52	-
LN3	1000	0.00	21.54	0.00	21.54	-
LN4	1400	0.00	21.56	0.00	21.56	-
LN5	1800	0.00	21.57	0.00	21.57	-
LN6	2200	0.00	21.58	0.00	21.58	-
LN7	2600	0.00	21.58	0.00	21.58	-
LN8	3000	0.00	21.60	0.00	21.60	-
LN9	3400	0.00	21.62	0.00	21.62	-
LN10	3800	0.00	21.63	0.00	21.63	-
	4000		21.65			
Average		**0.00**		**0.00**	**21.60**	**-**

Table 30: Wet probability P_w, mean free-surface elevation $\overline{\eta}$ (cm) and free-surface standard deviation σ_η (cm) at WG8 for N test series, SWL = 4 cm

Run	***t (s)***	P_w	z_b ***(cm)***	$\overline{h}$ ***(cm)***	$\overline{\eta}$ ***(cm)***	σ_η ***(cm)***
	0		21.65			
MN1	200	0.00	21.55	0.00	21.55	0.00
MN2	600	0.00	21.35	0.00	21.35	0.00
MN3	1000	0.007	21.14	0.008	21.15	0.068
MN4	1400	0.010	20.93	0.16	21.09	0.064
MN5	1800	0.011	20.72	0.14	20.86	0.051
MN6	2200	0.010	20.61	0.16	20.77	0.041
MN7	2600	0.006	20.50	0.17	20.67	0.036
MN8	3000	0.007	20.28	0.13	20.41	0.050
MN9	3400	0.007	20.06	0.14	20.20	0.036
MN10	3800	0.010	19.89	0.12	20.01	0.046
	4000		19.82			
Average		**0.0061**		**0.10**	**20.81**	**0.04**

Table 31: Wet probability P_w, mean free-surface elevation $\overline{\eta}$ (cm) and free-surface standard deviation σ_η (cm) at WG8 for N test series, SWL = 8 cm

Run	***t (s)***	P_w	z_b ***(cm)***	$\overline{h}$ ***(cm)***	$\overline{\eta}$ ***(cm)***	σ_η ***(cm)***
	0		19.82			
HN1	200	0.54	19.36	1.62	20.98	0.95
HN2	600	0.54	18.44	1.62	20.06	0.95
HN3	1000	0.54	17.52	1.66	19.18	0.95
HN4	1400	0.62	16.60	1.51	18.11	1.09
HN5	1800	0.65	15.68	1.64	17.32	1.19
HN6	2200	0.54	14.76	1.62	16.38	0.95
HN7	2600	0.71	13.84	1.84	15.68	1.28
HN8	3000	0.73	12.92	2.00	14.92	1.35
HN9	3400	0.76	12.00	2.03	14.03	1.40
HN10	3800	0.76	11.08	2.15	13.23	1.43
	4000		10.49			
Average		**0.64**		**1.77**	**17.00**	**1.15**

Table 32: Wet probability P_w, mean free-surface elevation $\overline{\eta}$ (cm) and free-surface standard deviation σ_η (cm) at WG8 for R test series, SWL = 0 cm

Run	*t (s)*	P_w	z_b *(cm)*	$\overline{h}$ *(cm)*	$\overline{\eta}$ *(cm)*	σ_η *(cm)*
	0		22.00			
LR1	200	0.062	22.00	0.60	22.60	0.19
LR2	600	0.067	22.00	0.61	22.61	0.19
LR3	1000	0.041	22.00	0.28	22.28	0.11
LR4	1400	0.042	22.00	0.18	22.18	0.11
LR5	1800	0.054	22.00	0.28	22.28	0.06
LR6	2200	0.026	22.00	0.20	22.20	0.08
LR7	2600	0.035	22.00	0.22	22.22	0.07
LR8	3000	0.031	22.00	0.17	22.17	0.08
LR9	3400	0.050	22.00	0.18	22.18	0.07
LR10	3800	0.045	22.00	0.22	22.22	0.05
	4000		22.00			
Average		**0.050**		**0.30**	**22.30**	**0.10**

Table 33: Wet probability P_w, mean free-surface elevation $\overline{\eta}$ (cm) and free-surface standard deviation σ_η (cm) at WG8 for R test series, SWL = 4 cm

Run	***t (s)***	***P_w***	***z_b (cm)***	***$\overline{h}$ (cm)***	***$\overline{\eta}$ (cm)***	***σ_η (cm)***
	0		22.00			
MR1	200	0.080	21.92	0.19	22.11	0.22
MR2	600	0.085	21.84	0.19	22.03	0.22
MR3	1000	0.076	21.75	0.22	21.97	0.15
MR4	1400	0.053	21.68	0.32	22.00	0.27
MR5	1800	0.052	21.59	0.23	21.82	0.21
MR6	2200	0.034	21.52	0.20	21.72	0.14
MR7	2600	0.052	21.43	0.16	21.59	0.17
MR8	3000	0.046	21.36	0.20	21.56	0.16
MR9	3400	0.038	21.32	0.21	21.53	0.17
MR10	3800	0.051	21.27	0.21	21.48	0.15
	4000		21.26			
Average		**0.057**		**0.21**	**21.78**	**0.18**

Table 34: Wet probability P_w, mean free-surface elevation $\overline{\eta}$ (cm) and free-surface standard deviation σ_η (cm) at WG8 for R test series, SWL = 8 cm

Run	*t (s)*	P_w	z_b *(cm)*	$\overline{h}$ *(cm)*	$\overline{\eta}$ *(cm)*	σ_η *(cm)*
	0		21.26			
HR1	200	0.54	21.22	1.10	22.32	0.32
HR2	600	0.53	20.91	1.17	22.08	0.39
HR3	1000	0.57	20.55	1.93	22.48	0.42
HR4	1400	0.68	20.19	2.51	22.70	0.44
HR5	1800	0.66	19.83	2.90	22.73	0.41
HR6	2200	0.67	19.47	3.10	22.57	0.41
HR7	2600	0.68	19.11	3.20	22.31	0.38
HR8	3000	0.66	18.75	3.30	22.05	0.38
HR9	3400	0.71	18.39	3.55	21.94	0.39
HR10	3800	0.69	18.03	3.60	21.63	0.41
	4000		17.94			
Average		**0.64**		**2.64**	**21.78**	**0.40**

Table 35: Wet probability P_w, mean free-surface elevation $\overline{\eta}$ (cm) and free-surface standard deviation σ_η (cm) at WG8 for S test series, SWL = 0 cm

Run	*t (s)*	P_w	z_b *(cm)*	$\overline{h}$ *(cm)*	$\overline{\eta}$ *(cm)*	σ_η *(cm)*
	0		22.00			
LS1	200	0.030	22.00	0.17	22.17	0.07
LS2	600	0.036	22.00	0.19	22.19	0.07
LS3	1000	0.019	22.00	0.19	22.19	0.05
LS4	1400	0.026	22.00	0.17	22.17	0.07
LS5	1800	0.036	22.00	0.21	22.21	0.05
LS6	2200	0.026	22.00	0.20	22.20	0.05
LS7	2600	0.028	22.00	0.17	22.17	0.07
LS8	3000	0.020	22.00	0.18	22.18	0.05
LS9	3400	0.017	22.00	0.19	22.19	0.05
LS10	3800	0.011	22.00	0.18	22.28	0.05
	4000		22.00			
Average		**0.025**		**0.19**	**22.20**	**0.06**

Table 36: Wet probability P_w, mean free-surface elevation $\overline{\eta}$ (cm) and free-surface standard deviation σ_η (cm) at WG8 for S test series, SWL = 4 cm

Run	***t (s)***	P_w	z_b ***(cm)***	$\overline{h}$ ***(cm)***	$\overline{\eta}$ ***(cm)***	σ_η ***(cm)***
	0		22.00			
MS1	200	0.12	21.92	0.20	22.12	0.19
MS2	600	0.14	21.76	0.23	21.99	0.28
MS3	1000	0.17	21.60	0.37	21.97	0.58
MS4	1400	0.17	21.44	0.14	21.58	0.40
MS5	1800	0.14	21.28	0.42	21.70	0.37
MS6	2200	0.15	21.12	0.42	21.54	0.40
MS7	2600	0.16	20.96	0.32	21.28	0.36
MS8	3000	0.17	20.80	0.31	21.11	0.38
MS9	3400	0.20	20.64	0.29	20.93	0.40
MS10	3800	0.19	20.48	0.36	20.84	0.42
	4000		20.22			
Average		**0.16**		**0.31**	**21.50**	**0.38**

Table 37: Wet probability P_w, mean free-surface elevation $\overline{\eta}$ (cm) and free-surface standard deviation σ_η (cm) at WG8 for S test series, SWL = 8 cm

Run	***t (s)***	***P_w***	***z_b (cm)***	***$\overline{h}$ (cm)***	***$\overline{\eta}$ (cm)***	***σ_η (cm)***
	0		20.22			
HS1	200	0.44	19.94	1.12	21.06	0.85
HS2	600	0.53	19.38	1.25	20.63	0.91
HS3	1000	0.57	18.82	1.61	20.43	0.93
HS4	1400	0.62	18.26	1.53	19.79	0.96
HS5	1800	0.65	17.70	1.61	19.31	1.02
HS6	2200	0.67	17.14	1.58	18.72	1.05
HS7	2600	0.69	16.58	1.61	18.19	1.08
HS8	3000	0.70	16.02	1.88	17.90	1.14
HS9	3400	0.73	15.46	1.95	17.41	1.14
HS10	3800	0.74	14.90	2.15	17.05	1.19
	4000		14.67			
Average		**0.63**		**1.63**	**19.05**	**1.03**

Table 38: Mean cross-shore $\overline{u}$ and standard deviation σ_u of the 2D ADV co-located with WG4 at x = 8.30 m, Red Vectrino co-located with WG5 at x = 12.90 m and Blue Vectrino co-located with WG6 at x = 15.52 m for N test series, SWL = 0 cm

Run	2D ADV at WG4		Red Vectrino at WG5		Blue Vectrino at WG6	
	$\bar{u}$ (*cm/s*)	σ_u (*cm/s*)	$\bar{u}$ (*cm/s*)	σ_u (*cm/s*)	$\bar{u}$ (*cm/s*)	σ_u (*cm/s*)
LN1	-8.15	22.65	-3.99	16.17	-3.42	16.60
LN2	-7.53	21.88	-3.90	16.35	-3.71	17.14
LN3	-8.20	22.38	NR	NR	-3.44	16.30
LN4	-7.05	22.23	-3.88	16.24	NR	NR
LN5	-6.88	22.30	-3.95	16.38	-3.32	16.91
LN6	-7.46	22.38	-3.49	16.33	NR	NR
LN7	-6.72	22.38	-3.54	16.41	-3.43	16.74
LN8	-6.00	22.07	-2.89	17.95	-3.34	17.15
LN9	-6.86	21.90	-3.30	16.19	NR	NR
LN10	-6.51	22.08	-3.39	16.24	-3.18	17.27
Average	**-7.13**	**22.22**	**-3.60**	**16.30**	**-3.40**	**16.87**

NR implies "not reliable" data

Table 39: Mean cross-shore $\overline{u}$ and standard deviation σ_u of the 2D ADV co-located with WG4 at x = 8.30 m, Red Vectrino co-located with WG5 at x = 12.90 m and Blue Vectrino co-located with WG6 at x = 15.52 m for N test series, SWL = 4 cm

Run	2D ADV at WG4		Red Vectrino at WG5		Blue Vectrino at WG6	
	$\bar{u}$ (*cm/s*)	σ_u (*cm/s*)	$\bar{u}$ (*cm/s*)	σ_u (*cm/s*)	$\bar{u}$ (*cm/s*)	σ_u (*cm/s*)
MN1	NR	NR	-4.37	17.68	-4.73	18.21
MN2	-5.49	23.70	-3.66	17.04	-4.37	18.30
MN3	-5.69	21.00	-3.36	17.07	-4.32	18.81
MN4	-5.60	21.04	-3.11	17.25	-4.10	18.57
MN5	-5.69	21.66	-3.53	17.41	-3.83	19.16
MN6	-5.56	21.67	-4.10	17.35	-3.97	19.38
MN7	-5.63	21.42	-3.90	17.44	-3.77	19.21
MN8	-5.58	21.28	-3.95	17.85	-3.74	19.15
MN9	-5.57	21.31	-3.82	17.21	-3.81	18.92
MN10	-5.66	21.62	-4.39	17.18	-3.87	19.02
Average	**-5.60**	**21.63**	**-3.81**	**17.30**	**-4.05**	**18.87**

NR implies "not reliable" data

Table 40: Mean cross-shore $\overline{u}$ and standard deviation σ_u of the 2D ADV co-located with WG4 at x = 8.30 m, Red Vectrino co-located with WG5 at x = 12.90 m and Blue Vectrino co-located with WG6 at x = 15.52 m for N test series, SWL = 8 cm

Run	2D ADV at WG4		Red Vectrino at WG5		Blue Vectrino at WG6	
	$\bar{u}$ (*cm/s*)	σ_u (*cm/s*)	$\bar{u}$ (*cm/s*)	σ_u (*cm/s*)	$\bar{u}$ (*cm/s*)	σ_u (*cm/s*)
HN1	-4.31	18.60	-3.49	20.61	-3.78	19.21
HN2	-4.41	20.80	-1.00	19.91	-5.08	23.96
HN3	-4.35	21.66	-3.54	20.05	-4.02	18.38
HN4	-4.88	23.69	-3.56	17.94	-3.81	18.16
HN5	-4.20	20.00	-3.39	17.98	-4.70	22.16
HN6	-4.29	24.15	-3.70	24.22	-3.09	23.24
HN7	-4.53	18.50	-3.53	17.75	-4.15	17.81
HN8	-4.26	17.99	-4.05	17.83	-3.71	17.81
HN9	-4.01	18.23	-3.28	17.71	-3.60	17.51
HN10	-4.24	17.73	-2.55	19.59	-3.74	17.53
Average	**-4.35**	**20.13**	**-3.21**	**19.75**	**-3.96**	**19.57**

NR implies "not reliable" data

Table 41: Mean cross-shore $\overline{u}$ and standard deviation σ_u of the 2D ADV co-located with WG4 at x = 8.30 m, Red Vectrino co-located with WG5 at x = 12.90 m and Blue Vectrino co-located with WG6 at x = 15.52 m for R test series, SWL = 0 cm

Run	2D ADV at WG4		Red Vectrino at WG5		Blue Vectrino at WG6	
	$\overline{u}$ (*cm/s*)	σ_u (*cm/s*)	$\overline{u}$ (*cm/s*)	σ_u (*cm/s*)	$\overline{u}$ (*cm/s*)	σ_u (*cm/s*)
LR1	-5.17	18.29	-4.93	16.07	-3.82	16.39
LR2	-5.07	18.36	-4.93	17.22	-3.88	16.70
LR3	-5.19	17.99	-3.03	16.13	-3.59	16.72
LR4	-5.01	18.06	-5.13	17.26	-3.79	16.87
LR5	-5.26	19.83	-2.37	16.26	-4.06	17.18
LR6	-5.06	21.45	-3.16	16.38	-3.63	17.18
LR7	-5.23	20.12	-3.01	16.32	-4.19	17.00
LR8	-5.30	14.61	-4.55	17.55	-4.22	17.11
LR9	-5.58	23.55	-2.77	16.74	NR	NR
LR10	NR	NR	-2.93	16.64	-4.00	17.27
Average	**-5.20**	**19.14**	**-3.68**	**16.53**	**-3.91**	**16.93**

NR implies "not reliable" data

Table 42: Mean cross-shore $\overline{u}$ and standard deviation σ_u of the 2D ADV co-located with WG4 at x = 8.30 m, Red Vectrino co-located with WG5 at x = 12.90 m and Blue Vectrino co-located with WG6 at x = 15.52 m for R test series, SWL = 4 cm

Run	2D ADV at WG4		Red Vectrino at WG5		Blue Vectrino at WG6	
	$\overline{u}$ (*cm/s*)	σ_u (*cm/s*)	$\overline{u}$ (*cm/s*)	σ_u (*cm/s*)	$\overline{u}$ (*cm/s*)	σ_u (*cm/s*)
MR1	-5.73	21.78	-3.72	17.42	NR	NR
MR2	-6.17	22.19	-3.59	17.61	-3.65	18.29
MR3	-6.24	22.64	-3.94	17.70	-3.69	18.59
MR4	-6.24	22.63	-5.48	20.88	-3.47	18.74
MR5	-7.62	22.86	-5.73	20.61	-3.96	18.52
MR6	-7.68	22.82	-4.06	17.92	-3.19	18.54
MR7	-6.28	22.76	-3.47	17.84	-3.66	18.76
MR8	-7.36	22.48	-4.06	17.65	-3.83	18.75
MR9	-6.29	22.31	-3.57	17.87	-3.56	18.76
MR10	-5.60	22.64	-3.49	17.81	-3.51	18.81
Average	**-6.52**	**22.51**	**-4.11**	**18.47**	**-3.61**	**18.64**

NR implies "not reliable" data

Table 43: Mean cross-shore $\overline{u}$ and standard deviation σ_u of the 2D ADV co-located with WG4 at x = 8.30 m, Red Vectrino co-located with WG5 at x = 12.90 m and Blue Vectrino co-located with WG6 at x = 15.52 m for R test series, SWL = 8 cm

Run	2D ADV at WG4		Red Vectrino at WG5		Blue Vectrino at WG6	
	$\overline{u}$ (*cm/s*)	σ_u (*cm/s*)	$\overline{u}$ (*cm/s*)	σ_u (*cm/s*)	$\overline{u}$ (*cm/s*)	σ_u (*cm/s*)
HR1	-4.29	22.41	-4.13	23.45	NR	NR
HR2	-4.44	22.70	-4.06	20.33	NR	NR
HR3	-5.19	23.13	-3.03	19.11	-3.36	19.59
HR4	-4.55	23.00	-3.97	18.89	-3.46	18.94
HR5	-4.94	23.41	-4.40	18.64	-2.97	19.64
HR6	-4.37	23.28	-3.86	18.58	-3.05	19.57
HR7	-4.72	23.06	-4.10	18.60	-3.14	19.55
HR8	-4.39	22.92	-3.93	18.86	-3.08	18.96
HR9	-4.85	22.85	-4.28	18.80	-2.96	19.70
HR10	-4.87	22.80	-3.32	19.86	-3.22	19.54
Average	**-4.66**	**22.95**	**-3.91**	**19.68**	**-3.15**	**19.44**

NR implies "not reliable" data

Table 44: Mean cross-shore $\overline{u}$ and standard deviation σ_u of the 2D ADV co-located with WG4 at x = 8.30 m, Red Vectrino co-located with WG5 at x = 12.90 m and Blue Vectrino co-located with WG6 at x = 15.52 m for S test series, SWL = 0 cm

Run	2D ADV at WG4		Red Vectrino at WG5		Blue Vectrino at WG6	
	$\overline{u}$ (*cm/s*)	σ_u (*cm/s*)	$\overline{u}$ (*cm/s*)	σ_u (*cm/s*)	$\overline{u}$ (*cm/s*)	σ_u (*cm/s*)
LS1	-6.27	20.84	-3.10	16.03	-3.97	16.10
LS2	-7.74	21.11	-3.30	15.87	-3.60	16.59
LS3	-8.23	20.83	-3.95	15.96	-3.42	16.33
LS4	-7.42	20.95	-3.15	19.27	-3.50	16.70
LS5	-7.20	20.82	-3.09	16.05	-3.60	16.04
LS6	-7.17	20.80	-3.14	16.47	-3.63	16.18
LS7	-7.16	20.84	-3.87	19.76	-3.92	16.89
LS8	-7.29	20.67	-2.81	16.33	-3.11	16.85
LS9	-7.68	20.71	-3.36	16.24	-3.33	16.52
LS10	-7.08	20.63	-3.71	16.18	-3.47	16.49
Average	**-7.32**	**20.82**	**-3.45**	**16.94**	**-3.55**	**16.47**

NR implies "not reliable" data

Table 45: Mean cross-shore $\overline{u}$ and standard deviation σ_u of the 2D ADV co-located with WG4 at x = 8.30 m, Red Vectrino co-located with WG5 at x = 12.90 m and Blue Vectrino co-located with WG6 at x = 15.52 m for S test series, SWL = 4 cm

Run	2D ADV at WG4		Red Vectrino at WG5		Blue Vectrino at WG6	
	$\overline{u}$ (*cm/s*)	σ_u (*cm/s*)	$\overline{u}$ (*cm/s*)	σ_u (*cm/s*)	$\overline{u}$ (*cm/s*)	σ_u (*cm/s*)
MS1	-6.89	21.56	-3.69	20.84	-3.21	19.12
MS2	-7.00	21.26	-3.75	19.72	-3.37	19.00
MS3	-7.34	21.19	-3.41	17.61	-3.40	19.04
MS4	-7.50	21.03	-3.60	17.61	-2.84	19.05
MS5	-7.43	21.00	-3.99	17.54	-3.67	19.02
MS6	-6.86	21.19	-3.55	17.65	NA	NA
MS7	-7.39	20.76	-3.67	17.66	-3.52	19.19
MS8	-7.23	20.94	-2.83	17.75	-3.09	18.95
MS9	-7.72	20.51	-3.66	17.61	-3.67	19.01
MS10	-6.78	20.75	-3.71	16.18	-3.47	16.49
Average	**-7.21**	**21.14**	**-3.58**	**18.10**	**-3.36**	**18.76**

NR implies "not reliable" data

Table 46: Mean cross-shore $\overline{u}$ and standard deviation σ_u of the 2D ADV co-located with WG4 at x = 8.30 m, Red Vectrino co-located with WG5 at x = 12.90 m and Blue Vectrino co-located with WG6 at x = 15.52 m for S test series, SWL = 8 cm

Run	2D ADV at WG4		Red Vectrino at WG5		Blue Vectrino at WG6	
	$\overline{u}$ (*cm/s*)	σ_u (*cm/s*)	$\overline{u}$ (*cm/s*)	σ_u (*cm/s*)	$\overline{u}$ (*cm/s*)	σ_u (*cm/s*)
HS1	-4.25	20.67	-4.29	19.86	-2.84	20.94
HS2	-3.05	19.48	-3.15	19.78	-2.39	18.86
HS3	-4.64	21.36	-2.08	20.27	-3.11	19.43
HS4	-4.50	20.83	-4.13	19.49	-3.43	19.42
HS5	-4.87	21.44	-4.17	18.75	-3.57	19.05
HS6	-5.24	21.28	-3.87	20.04	-3.81	19.04
HS7	-3.87	21.10	-3.81	18.30	-3.30	18.95
HS8	-6.19	21.36	-4.23	18.71	-3.18	19.22
HS9	-4.89	21.48	-3.98	18.27	-3.53	19.12
HS10	-4.70	21.25	-4.56	18.66	-3.31	18.86
Average	**-4.62**	**21.03**	**-3.82**	**19.40**	**-3.24**	**19.28**

NR implies "not reliable" data

Figure 5 shows the average values of the mean $\overline{\eta}$, standard deviation σ_η, wet probability P_w, mean $\overline{u}$, and standard deviation σ_u for 10 runs with the 4-cm SWL in the N, R, and S tests. The sum of $\overline{\eta}$ and SWL (4 cm) is the mean water level above the datum $z = 0$. The measured values of $\overline{\eta}$ were slightly negative (wave setdown) at WG1 – WG3 outside the surf zone and WG4 at x = 8.3 m near the breaker zone. The values of $\overline{\eta}$ were positive (wave setup) at WG5 – WG7 located at x= 12.9, 15.5, and 17.1 m in the inner surf zone. The sum of $\overline{\eta}$ and SWL at WG8 (x = 18.6 m) equals the sum of the bottom elevation at WG8 and the measured mean depth which was less than 0.3 cm. The bottom elevation changes during the 4-cm SWL were relatively small and the average

values plotted in Figure 5 represented the measured ten values in each test. The sill was located in the zone of x = 16.16 – 16.64 m seaward of WG7. Wave setup landward of the sill was expected to be noticeable in light of previous laboratory experiments [e.g. Kobayashi et al. (2007)] but the increase of $\overline{\eta}$ attributable to the sill was less than 0.2 cm perhaps because of its narrow width. Wave setup was much smaller than the SWL increase of 4 and 8 cm in this experiment.

The second panel for the free surface standard deviation σ_η in Figure 5 shows the cross-shore variation of the local significant wave height, 4 σ_η. The wave height decreased in the surf zone and became very small in the swash zone. The sill (S) was effective in reducing the value of σ_η at x = 17.1 m landward of the sill in the comparison to those for the N and R tests. The wet probability P_w was unity at WG1 – WG7 and small at WG8, indicating minor wave overtopping for the 4-cm SWL. The mean horizontal velocity $\overline{u}$ at x = 8.3, 12.9, and 15.5 m was negative because of the wave-induced offshore return current. The velocity standard deviation σ_u represents the intensity of the wave-induced oscillatory velocity. The return current and oscillatory velocity decreased from the breaker zone to the inner surf zone. The differences of $\overline{u}$ and σ_u at given x among the three tests may have been caused partly by the measurement error of about 1 cm/s.

Figure 6 presents the average values of mean and standard deviation of the free surface elevation η and wet probability P_w at WG6 – WG8 for 10 runs with SWL=0, 4 and 8 cm in the S test. The increase of SWL increased the wave height at WG6 – WG8 located inside the surf zone. Wave gauge WG8 at x=18.6 m on the berm crest became wetter as the SWL was increased and the berm was eroded.

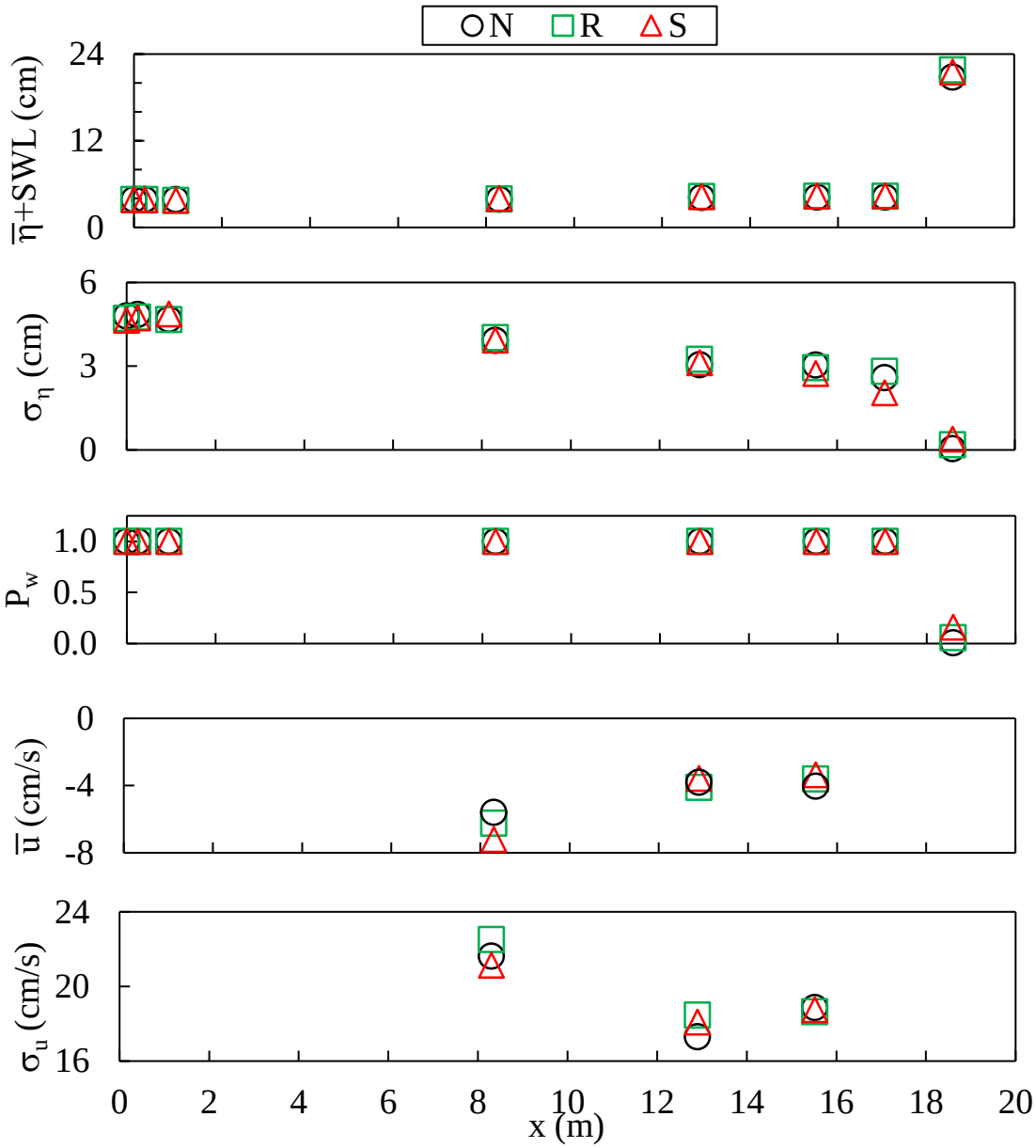

Figure 5: Average values of mean and standard deviation of free surface elevation η and horizontal velocity u together with wet probability P_w for 10 runs with 4-cm SWL for Tests N, R, and S

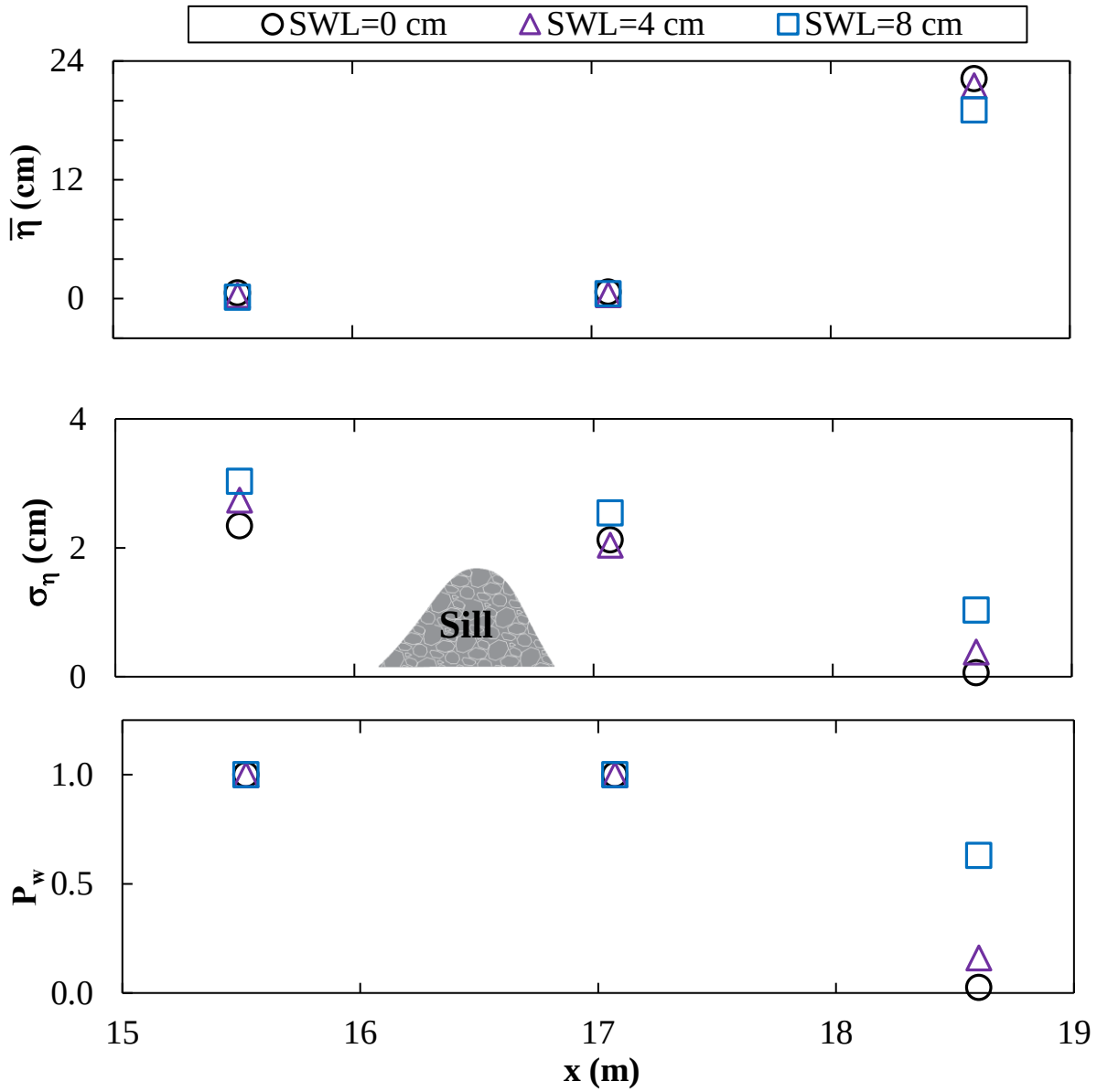

Figure 6: Average values of mean and standard deviation of free surface elevation η and wet probability P_w at WG6 – WG8 for 10 runs with SWL=0, 4 and 8 cm in Test S

3.2 Wave Overtopping and Overwash Rates

The measured volumes of water and sand transported over the impermeable vertical wall were used to obtain the water overtopping rate q_0 and sand overwash rate q_{bs} per unit width averaged over each 400-s run. The measured values are given in Tables 47 – 52.

Table 47: Measured sediment overwash rate (q_{bs}), water overtopping rate (q_o), and their ratio for N test series, SWL = 0 cm

Run	q_{bs} (cm^2/s)	q_o (cm^2/s)	q_{bs}/q_o
LN1	0.00	0.0073	0.00
LN2	0.00	0.0055	0.00
LN3	0.00	0.0011	0.00
LN4	0.00	0.0005	0.00
LN5	0.00	0.0038	0.00
LN6	0.00	0.0023	0.00
LN7	0.00	0.0050	0.00
LN8	0.00	0.0033	0.00
LN9	0.00	0.0016	0.00
LN10	0.00	0.0004	0.00

Table 48: Measured sediment overwash rate (q_{bs}), water overtopping rate (q_o), and their ratio for N test series, SWL = 4 cm

Run	q_{bs} (cm^2/s)	q_o (cm^2/s)	q_{bs}/q_o
MN1	0.00	0.0247	0.00
MN2	0.00	0.0046	0.00
MN3	0.00	0.0036	0.00
MN4	0.00	0.0252	0.00
MN5	0.00	0.0771	0.00
MN6	0.00	0.0823	0.00
MN7	0.00	0.0650	0.00
MN8	0.00	0.0814	0.00
MN9	0.00	0.0903	0.00
MN10	0.00	0.0950	0.00

Table 49: Measured sediment overwash rate (q_{bs}), water overtopping rate (q_o), and their ratio for N test series, SWL = 8 cm

Run	q_{bs} (cm^2/s)	q_o (cm^2/s)	q_{bs}/q_o
HN1	0.070	3.21	0.022
HN2	0.066	1.98	0.033
HN3	0.077	3.99	0.021
HN4	0.067	2.26	0.032
HN5	0.067	2.78	0.025
HN6	0.052	3.96	0.013
HN7	0.050	2.44	0.021
HN8	0.053	3.98	0.013
HN9	0.052	2.37	0.021
HN10	0.050	1.91	0.026

Table 50: Measured sediment overwash rate (q_{bs}), water overtopping rate (q_o), and their ratio for R test series, SWL = 8 cm

Run	q_{bs} (cm^2/s)	q_o (cm^2/s)	q_{bs}/q_o
HR1	0.0033	0.44	0.0075
HR2	0.0035	0.42	0.0083
HR3	0.0033	0.40	0.0082
HR4	0.0034	0.22	0.0151
HR5	0.0034	0.39	0.0087
HR6	0.0041	0.43	0.0094
HR7	0.0037	0.35	0.0105
HR8	0.0057	0.52	0.0110
HR9	0.0051	0.52	0.0098
HR10	0.0058	0.48	0.0118

Table 51: Measured sediment overwash rate (q_{bs}), water overtopping rate (q_o), and their ratio for

S test series, SWL = 4 cm

Run	q_{bs} (cm^2/s)	q_o (cm^2/s)	q_{bs}/q_o
MS1	0.00	0.0040	0.00
MS2	0.00	0.0106	0.00
MS3	0.00	0.0402	0.00
MS4	0.00	0.0530	0.00
MS5	0.00	0.0657	0.00
MS6	0.00	0.0795	0.00
MS7	0.00	0.0392	0.00
MS8	0.00	0.0473	0.00
MS9	0.00	0.0656	0.00
MS10	0.00	0.0461	0.00

Table 52: Measured sediment overwash rate (q_{bs}), water overtopping rate (q_o), and their ratio for S test series, SWL = 8 cm

Run	q_{bs} (cm^2/s)	q_o (cm^2/s)	q_{bs}/q_o
HS1	0.057	2.54	0.024
HS2	0.046	2.26	0.021
HS3	0.053	1.74	0.033
HS4	0.057	2.56	0.024
HS5	0.054	2.07	0.028
HS6	0.047	1.57	0.033
HS7	0.052	2.44	0.023
HS8	0.049	2.35	0.022
HS9	0.044	1.68	0.028
HS10	0.043	2.31	0.019

Figure 7 shows the temporal variations of q_0 and q_{bs} for all the runs in the N, R, and S tests. The data points with $q_0 = 0$ and $q_{bs} = 0$ are not shown in the logarithmic plotting. The average rates are plotted at time t corresponding to the middle of each run with $t=0$ at the start of each test. The SWL was increased by the 4-cm increment at t = 4,000 and 8,000 s. For the N test, minor wave overtopping occurred during t = 0 – 8,000 s but no sand overwash occurred because sand in the overtopped water was deposited on the 1.3-m wide berm between WG8 and the vertical wall (Figure 3). During t = 8,000 – 12,000 s, major wave overtopping with q_0 exceeding 2 cm^2/s (0.2 liter/s/m) occurred and the corresponding sand overwash rate q_{bs} was about 0.06 cm^2/s. For the R test, wave overtopping and overwash did not occur during t = 0 – 8,000 s. When the SWL was increased to 8 cm, the values of q_0 and q_{bs} were about 0.4 and 0.004 cm^2/s, respectively. The revetment reduced q_0 and q_{bs} considerably. For the S test, wave overtopping and overwash did not occur during t = 0 – 4,000 s. Minor wave overtopping occurred during t = 4,000 – 8,000 s but sand in the overtopped water did not reach the vertical wall. The values of q_0 and q_{bs} during t = 8,000 – 12,000 s became as large as those for the N test because the sill crest was sufficiently submerged as explained in the following.

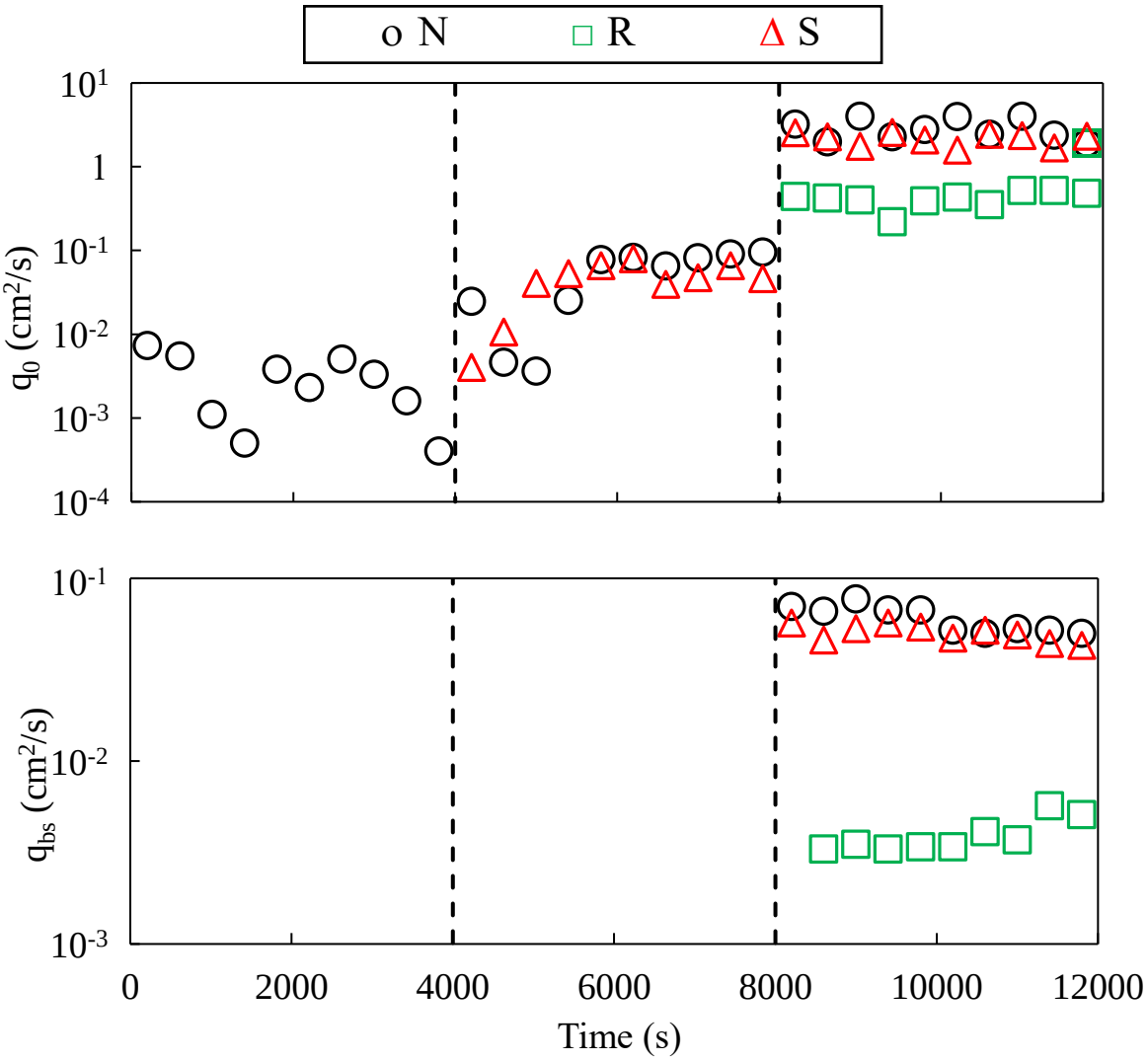

Figure 7: Temporal variations of wave overtopping rate (q_0) and sand overwash rate (q_{bs}) for Tests N, R, and S with 4-cm SWL increase at time 4,000 and 8,000 s

3.3 Profile Evolution

The profile evolution of the N test is shown in Figure 8 where use is made of t_1 = 4,000 s, t_2 = 8,000 s, and t_3 = 12,000 s for brevity. The SWL was increased by the increment of 4 cm at t = t_1 and t_2. The SWL shoreline at t = 0 was located on the gentle beach in front of the steep slope of the initial (t = 0) profile. The profiles in the zone of x = 15.0 – 19.9 m of noticeable profile changes are presented for clarity. Onshore sand transport and accretion in front of the steep slope occurred during t = 0 – t_1 perhaps because the initial profile was created by moving sand offshore from the accreted zone as explained in relation to Figure 4. During t = t_1 – t_2 with the 4-cm SWL, the profile change was relatively small and minor wave overtopping eroded the upper part of the steep slope. During t = t_2 – t_3 with the 8-cm SWL, the steep slope was eroded significantly and became gentler under major wave overtopping. The values of q_0 and q_{bs} in Figure 7 did not change much during t = t_2 – t_3.

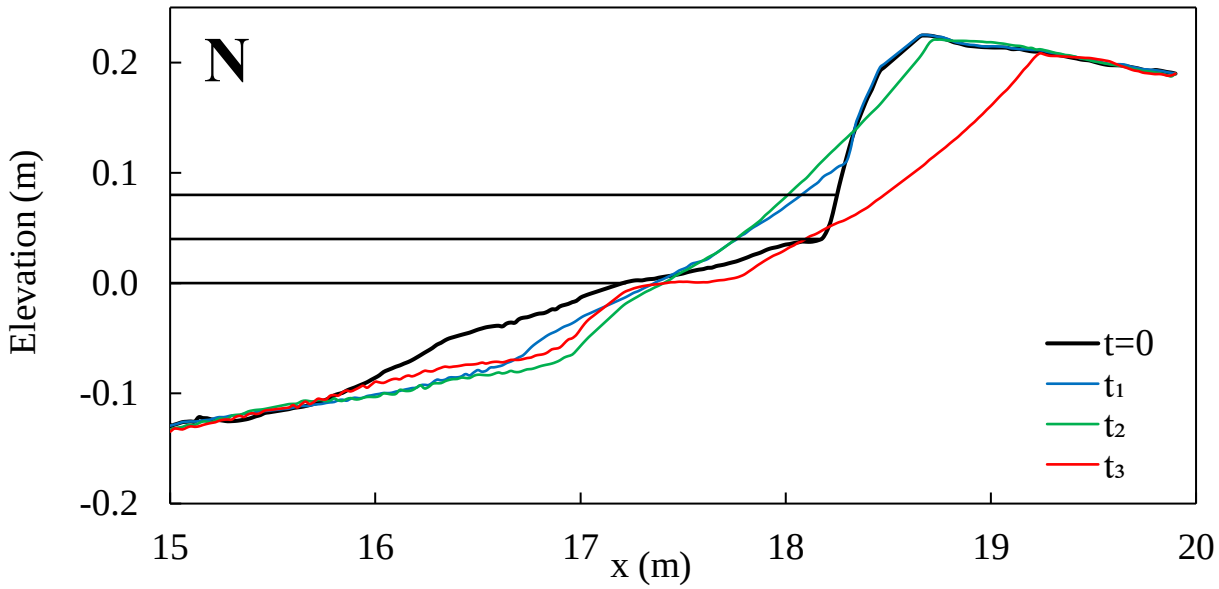

Figure 8: Measured profiles for Test N at time t = 0, t_1 = 4,000 s, t_2 = 8,000 s, and t_3 = 12,000 s with 4-cm SWL increase at t_1 and t_2

Figure 9 shows the measured profiles at $t = 0$, t_1, t_2 and t_3 for the R test where the revetment was situated in the zone of x = 18.12 – 18.52 m. During $t = 0 - t_1$, onshore sand transport and accretion occurred in front of the revetment. The toe of the revetment was located 8-cm above the initial SWL. During $t = t_1 - t_2$, minor erosion occurred above the 4-cm SWL and below the revetment toe. The erosion and accretion patterns during $t = 0 - t_2$ for the N and R tests were similar when the effect of the revetment on sand transport in the swash zone was relatively small. It should be noted that the initial profile near the SWL of 0 and 4-cm was gentler for the N test than for the R test. During $t = t_2 - t_3$ with the 8-cm SWL, wave overtopping caused scour landward of the revetment crest and dislodged stones placed loosely on the smooth fabric mesh. The revetment was damaged but shore erosion above the initial SWL was less in the R test than in the N test.

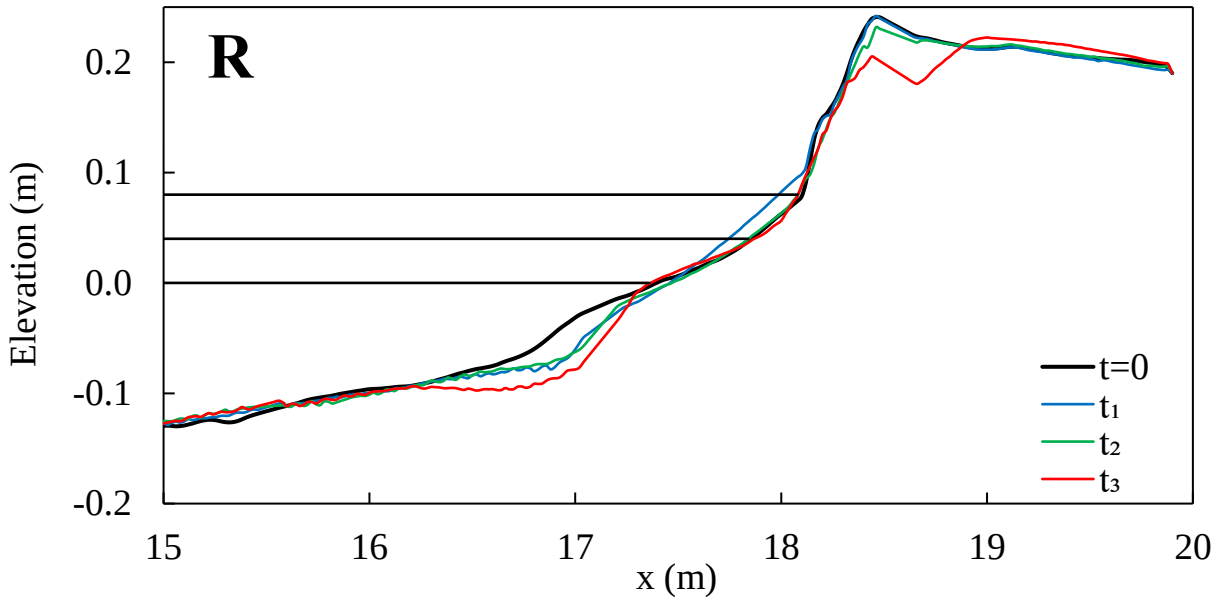

Figure 9: Measured profiles for Test R at time $t = 0$, t_1 = 4,000 s, t_2 = 8,000 s, and t_3 = 12,000 s with 4-cm SWL increase at t_1 and t_2

The measured profiles for the S test are shown in Figure 10 where the sill was located in the zone of x = 16.16 – 16.64 m. During $t = 0 - t_1$, the sill crest located 4.1 cm above the SWL at $t=0$ was damaged and lowered by 2.6 cm by $t = t_1$. The sand profile change was small apart from minor scour at the seaward sill toe and localized erosion below the initial SWL. During $t = t_1 - t_2$ with the 4-cm SWL, the sill crest was submerged and the sill profile did not change much. The sand profile change was limited to the zone landward of the sill. The erosion and accretion patterns during $t = t_1 - t_2$ were similar for the N and S tests. During $t = t_2 - t_3$ with the 8-cm SWL, the still water depth above the sill was approximately 7 cm in comparison to the incident significant wave height H_{m0} = 19 cm. The similarity of the sand profile changes for the N and S tests became more apparent except for scour at the seaward sill toe. The narrow sill in this experiment was not effective in reducing shore erosion when it was submerged sufficiently (about 0.4 H_{m0} below the SWL).

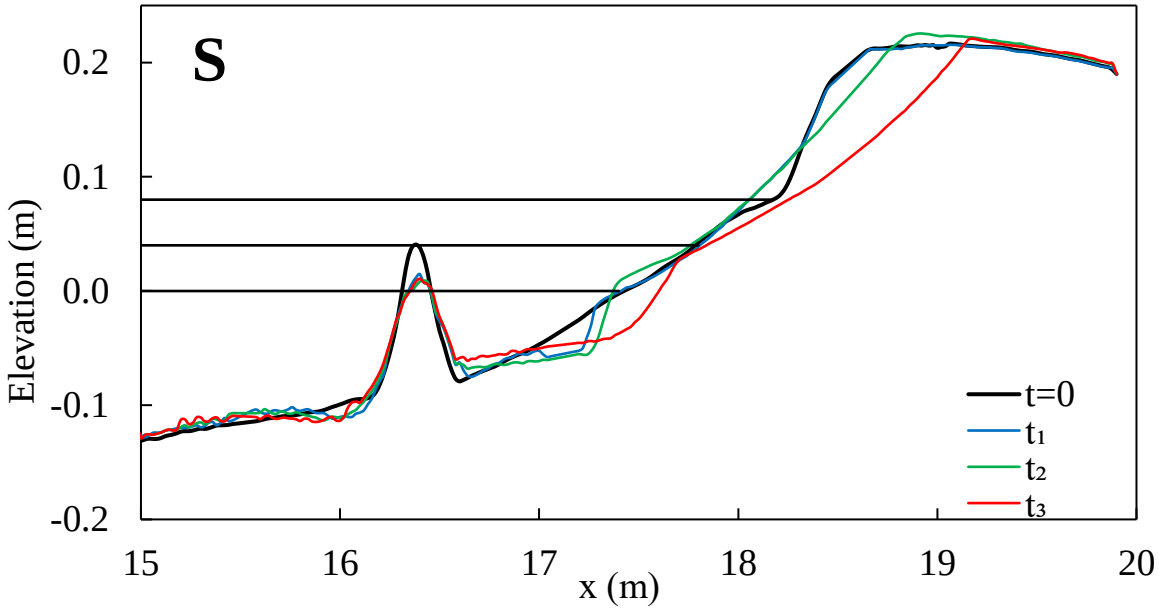

Figure 10: Measured profiles for Test S at time t = 0, t_1 = 4,000 s, t_2 = 8,000 s, and t_3 = 12,000 s with 4-cm SWL increase at t_1 and t_2

3.4 Damage Progression and Deposited Sand Height inside Porous Stone Structures

Damage progression of the stone revetment and sill was analyzed using a conventional method [e.g., Melby and Kobayashi (1998)]. The measured stone profiles at $t = 0$, t_1, t_2 and t_3 were compared with the initial stone profile to calculate the eroded (lowered) area A_e of the initial stone cross section. The green and blue stones were used in the experiment as explained in relation to Figure 4. The segments of the green and blue stones were averaged separately and the alongshore averaged profile for each segment was used to calculate A_e for each stone. Figure 11 shows the temporal variation of damage $S_e = A_e / (D_{n50})^2$, where the nominal diameter D_{n50} = 3.52 and 3.81 cm for the green and blue stones, respectively. The damage S_e starting from $S_e = 0$ at $t = 0$ increased with time. The revetment damage progression was related to the increase of wave action on the revetment with the 4-cm increment of the SWL at t = 4,000 and 8,000 s, where the damage was negligible during t = 0 – 4,000 s with the initial SWL. The sill damage progression was related to wave action on the sill crest. The narrow (about two-stone width) sill crest emerged 4.1 cm (about one-stone height) above the initial SWL was damaged during t = 0 – 4,000 s but the damaged crest was submerged and fairly stable under the SWL of 4 – 8 cm during t= 4,000 – 12,000 s. The damage difference between the green and blue stones was caused partly by the nominal diameter difference of 8% and partly by the alongshore variability of the eroded area which was investigated by Melby and Kobayashi (1998).

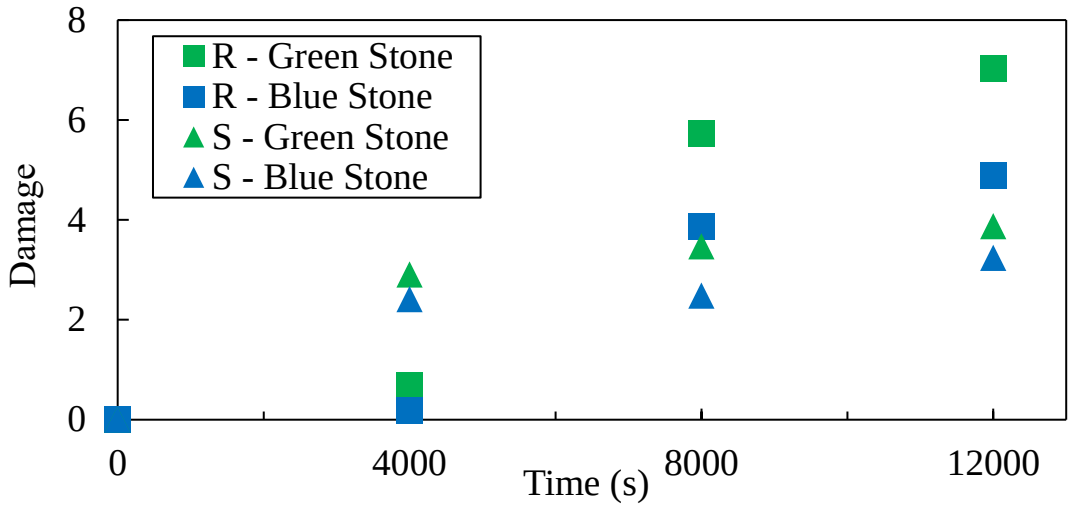

Figure 11: Damage progression of green and blue stones in Tests R and S

The cause of the stone damage was examined in the same way as in the stone seawall experiment by Kobayashi and Kim (2017). The initial and final profiles of the stone surface and fabric mesh filter for the R and S tests are shown in Figure 12. The cross-shore variations of the revetment erosion depth and the filter settlement depth in the R test indicated that the revetment damage in Figure 11 was caused mostly by the filter settlement. Wave overtopping caused additional damage on the revetment crest. Some of the stones on the revetment crest were dislodged landward onto the sand surface and the filter was visible at locations of stone dislodgement. For the S test, the initial and final filter elevations were essentially the same and the filter settlement did not occur. The stones dislodged from the sill crest were deposited on the side slopes. The damaged crest shifted landward probably because of onshore stone movement under breaking wave action over the low and narrow crest. Some stones moved seaward during wave downrush on the seaward slope. Finally, the deposited sand height on the filter was about 0.3 and 0.8 cm inside the revetment and sill, respectively, where no sand existed on the filter at the beginning of each test (Figure 13).

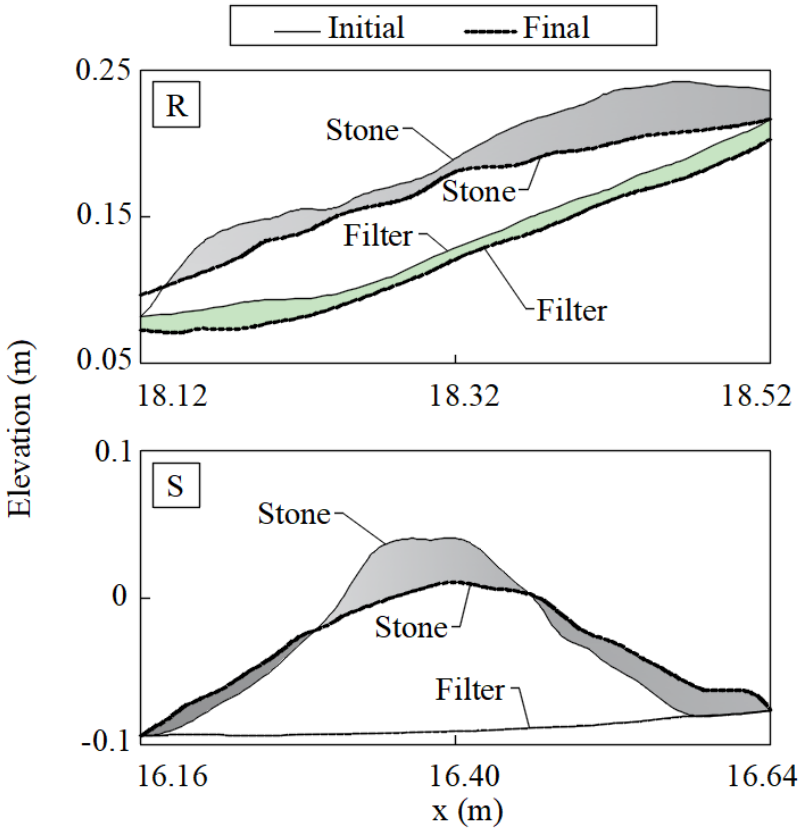

Figure 12: Settlement of stone surface and filter from time $t = 0$ to $t_3 = 12{,}000$ s for Tests R and S

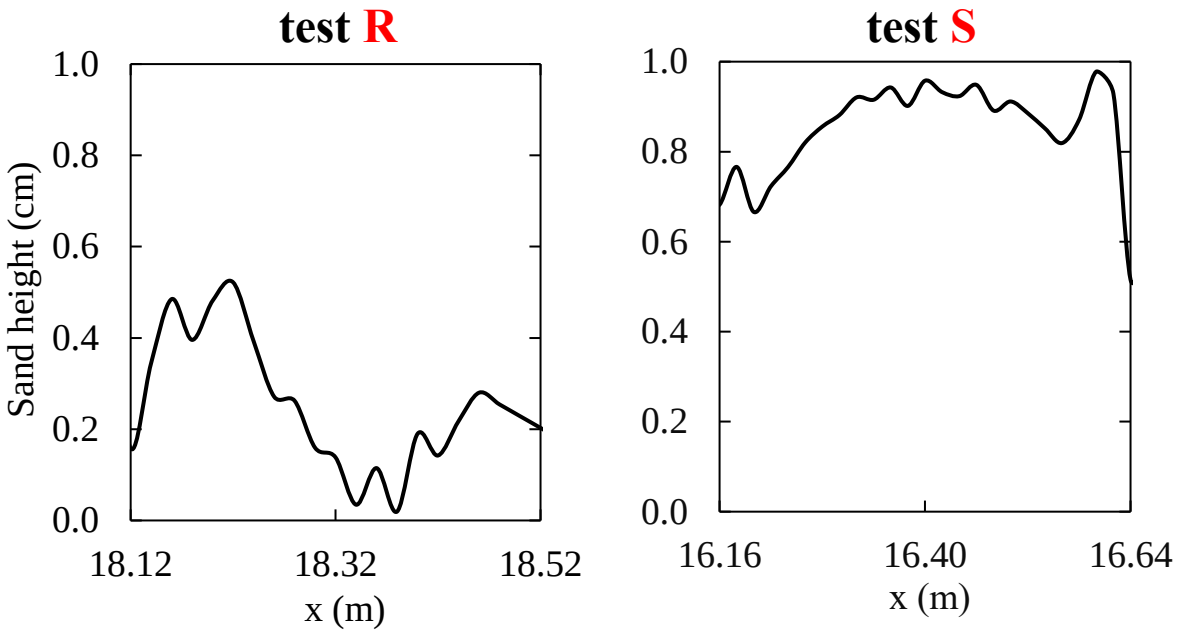

Figure 13: Deposited sand height inside porous revetment and sill structures

Chapter 4

NUMERICAL MODEL

4.1 Cross – Shore Model (CSHORE)

The small-scale laboratory tests compared the revetment and sill in terms of their efficacies in reducing shore erosion and wave overtopping under limited conditions. A process-based numerical model is required to design the revetments and sill for various prototype conditions. Kobayashi (2016) reviewed the capabilities and shortcomings of phase-averaged and resolving models. The phase-averaged model CSHORE was upgraded because of its versatility and computational efficiency. The version of CSHORE used in the comparisons included the following components: a combined wave and current model based on time-averaged continuity, momentum, wave action, and roller energy equations; a sediment transport model for bed load and suspended load coupled with the continuity equation of bottom sediment; a permeable layer model for porous flow; and a probabilistic swash model on impermeable (fine sand) and permeable (stone) bottoms. The measured values of $\overline{\eta}$, H_{m0}, and T_p at $x = 0$ for 30 runs in each test were specified as input. The nodal spacing was 2 cm. The input parameters for CSHORE were taken as standard values because the degree of overall agreement for the 3 tests did not improve without calibrating each parameter for each test.

No upgrading of CSHORE was necessary for the comparison with the N test with no stone structure which is similar to the tests for wave overtopping and overwash of dunes conducted by Figlus et al. (2011) in the same wave flume. The comparison with the revetment (R) test was made using the CSHORE option added by Kobayashi and Kim (2017) for their stone seawall tests

conducted in the same wave flume. This option allows the computation of sand transport on and inside a stone structure placed on a fixed filter. The sand, stones, and filter in their experiment were used in the present experiment. The assumption of the fixed filter is appropriate for the S test but neglects the filter settlement in the R test (Figure 12). As a result, an option for no filter was added in the upgraded CSHORE to allow erosion of sand below the filter. For the fixed filter option, sand erosion inside the porous structure was limited by available sand above the fixed filter as explained in the formulation by Kobayashi and Kim (2017). For the no filter option, sand below the filter is eroded if available sand is limited. Sand erosion below the filter results in the filter and stone settlement where the stone layer thickness is assumed invariant. The no filter option may be regarded to represent a stone structure placed on sand directly. It should be noted that sand below the filter may also be transported along the filter. Both filter options neglect sand migration below and along the filter.

CSHORE was modified for the comparison with the sill (S) test. Kobayashi et al. (2013) extended CSHORE to the zone of wave transmission landward of an emerged stone structure. The extended CSHORE was compared with 148 reef breakwater tests by Ahrens (1989). Garcia and Kobayashi (2015) compared it with 188 low-crested (emerged and submerged) breakwater tests. These comparisons were limited to damage and wave transmission coefficient data for stone structures located on fixed horizontal bottoms. The emerged sand beach landward of the emerged or submerged sill in the S test needs to be included in the computation domain. The S test is similar to the two tests conducted by Figlus et al. (2012) for a ridge and a runnel in the same wave flume. The stone sill and the sand ridge were emerged initially. The sill became submerged subsequently and the emerged sand ridge migrated onshore into the ponded runnel. The

CSHORE option for an emerged impermeable ridge and a ponded runnel was developed by Figlus et al. (2012) using their two tests. This option has been upgraded to allow for porous flow through an emerged or submerged stone structure.

4.2 Comparison with Three Tests

The present CSHORE cannot predict sand beach evolution and stone structure damage simultaneously. Damage on the stone revetment and sill was computed assuming no deformation of the initial sand beach profile. Garcia and Kobayashi (2015) calibrated two input parameters using 104 tests for the prediction of damage on low-crested stone breakwaters. The critical stability number N_c related to the instantaneous fluid velocity for initiation of stone movement (Kobayashi et al. 2010) was calibrated as $N_c = 0.6$. Stones piled on the narrow sill crest in the S test were found to be exceptionally unstable perhaps because of insufficient contact with neighboring stones. Figure 14 shows the computed damage progression with $N_c = 0.1$ for the blue and green stones in the S test in comparison with the measured damage in Figure 11. The computed damage is plotted at the end of each 400-s run starting from zero damage at time $t = 0$. The calibrated value of $N_c = 0.1$ gave good agreement at $t = 12{,}000$ s but underpredicted damage at $t = 4{,}000$ s probably because of the spatial variation of N_c over the sill. The damage progression for the S test was predicted within errors of 100 %. For the R test, the computed damage at $t = 12{,}000$ s was 0.45 and 0.67 for the blue and green stones, respectively. The computed damage for the R test was much smaller than the measured damage in Figure 11, partly because of the filter settlement (Figure 12).

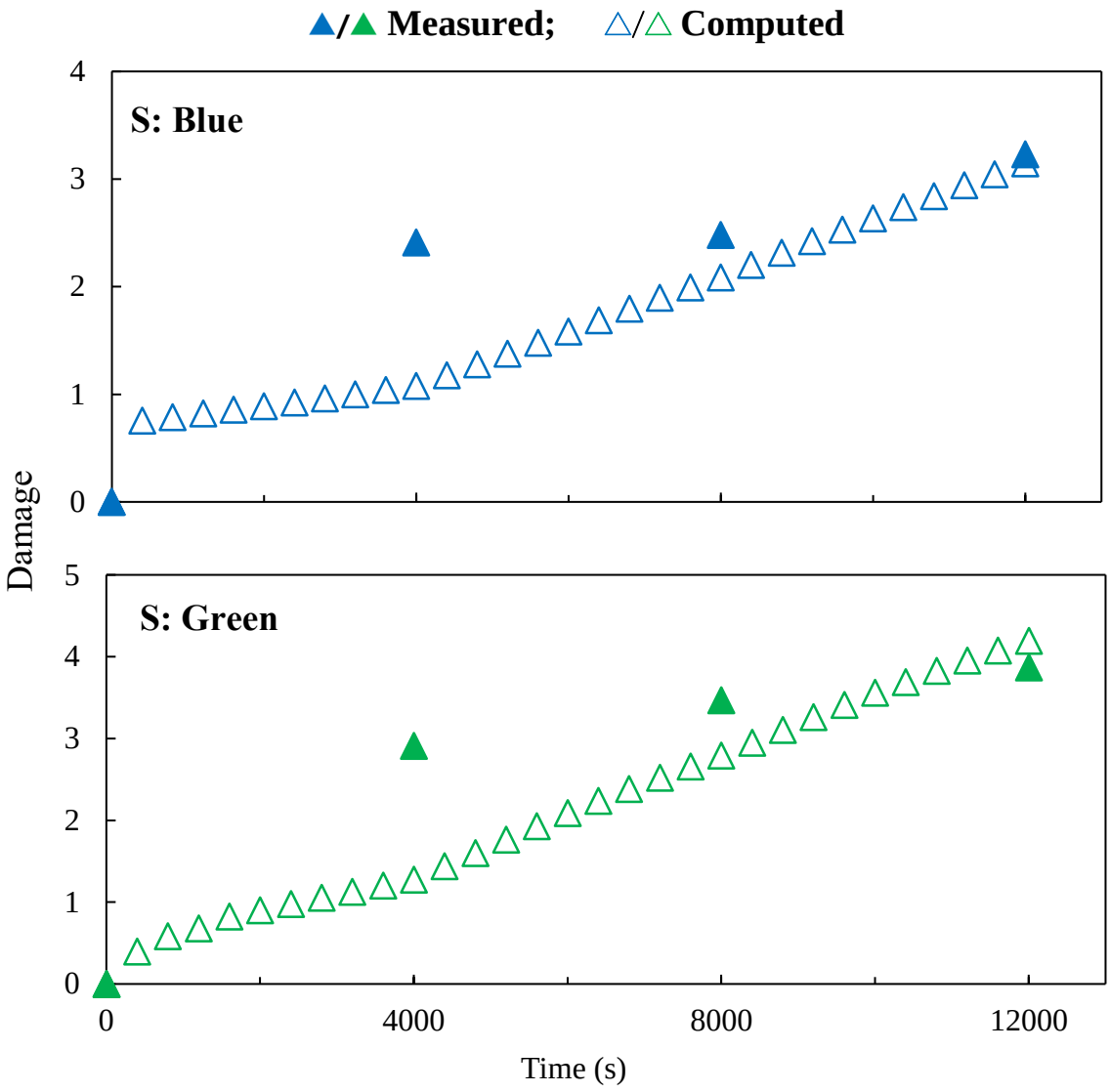

Figure 14: Computed and measured damage of blue and green stones in Test S

For the computation of sand beach profile evolution in the N, R, and S tests, the measured initial profile was specified as input. The stones in the R and S tests were assumed to be immobile on the filter, which was assumed to be fixed. An average nominal diameter D_{50} = 3.65 cm was used for the green and blue stones, accounting for the stone width difference. Computation was also made using an adjusted initial profile for the R and S tests. The lower part of the seaward revetment

slope was lowered to make the adjusted slope resemble the settled and stabilized slope measured at time t = 8,000 and 12,000 s. The stone layer thickness was kept the same as the initial thickness. The adjusted sill profile was taken as the damaged and stabilized sill profile measured at t = 4,000 s. These adjustments were regarded to reduce errors caused by the assumptions of no settlement and no stone damage. The agreement for the adjusted initial profile was somewhat better than that for the original initial profile. The computed results in the following are based on the adjusted initial profiles for the R and S tests.

The computed and measured cross-shore variations of the mean and standard deviation of the free surface elevation η and horizontal velocity u together with the wet probability P_w for 10 runs with SWLs of 0, 4, and 8 cm were compared for the N, R, and S tests. The agreement for the N and R tests was similar to that for the similar tests by Kobayashi and Kim (2017). Figure 15 shows the comparison for 10 runs with the 8-cm SWL in the S test. The measured and computed values for the 10 runs were averaged and plotted so as to highlight the sill effect on the hydrodynamic variables. The sill was located in the zone of x = 16.16 – 16.64 m. Wave gauges WG6 and WG7 were located at x = 15.5 and 17.1 m, respectively. These hydrodynamic variables were predicted within errors of approximately 20 %, except for WG7 located immediately landward of the sill. The computed mean water level ($\overline{\eta}$ + SWL) above the datum z = 0 fluctuated over the sill. The values of σ_η at WG7 were underpredicted for all the runs in the S test perhaps because the wave breaking and roller model in CSHORE developed for beaches cannot adequately predict the breaking wave transformation over the narrow sill with steep side slopes. The value of σ_η at WG8 in the wet and dry zone (P_w < 1) was predicted within the expected error of 20 %, indicating the local nature of the error at WG7 immediately landward of the sill. The mean

horizontal velocity $\overline{u}$ was negative (offshore) in the zone dominated by the offshore return flow and positive (onshore) in the wet and dry zone dominated by wave overtopping flow. The computed offshore return current was large over this sill and on the relatively steep beach slope near the shoreline (Figure 10). The computed standard deviation σ_u of the wave-induced oscillatory velocity was large in the two zones of the large offshore current.

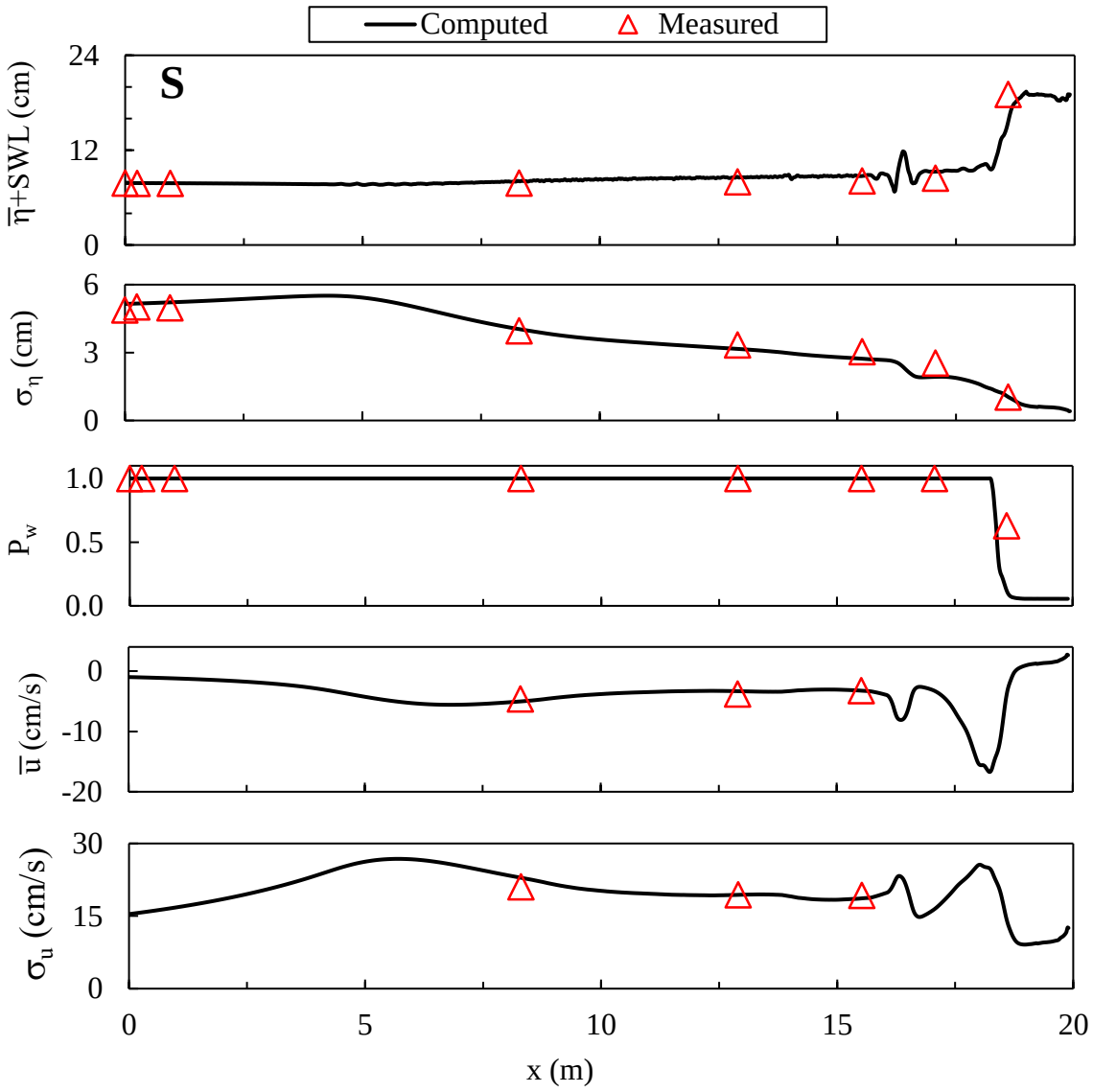

Figure 15: Computed and measured average values of mean and standard deviation of η and u together with P_w for 10 runs with 8-cm SWL for Test S

Figure 16 compares the average overtopping rate q_0 and overwash rate q_{bs} during each run for the N, R, and S tests, where the measured and computed points with $q_0 = 0$ and $q_{bs} = 0$ are not shown in the logarithmic plot of q_0 and q_{bs}. The measured small rates of q_0 of the order of 0.1 cm^2/s or less were not predicted by CSHORE partly because the landward limit of CSHORE computation was at the mean water depth of 0.01 cm or less. The small rates of q_{bs} of the order of 0.01 cm^2/s were not reproduced reasonable partly because CSHORE could not predict deposition of sand on the 1.3-m wide berm during minor wave overtopping. The larger rates of q_0 and q_{bs} were predicted within errors of about 100 %.

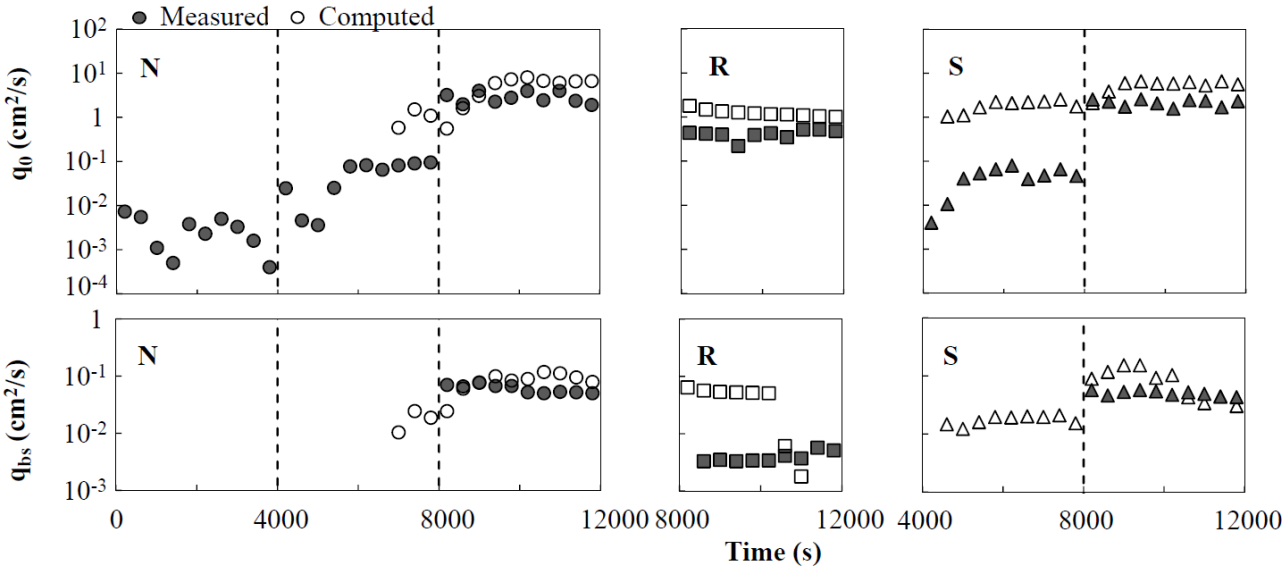

Figure 16: Comparison of computed and measured q_0 and q_{bs} for Tests N, R, and S

The measured and computed profiles at time $t_1 = 4{,}000$ s, $t_2 = 8{,}000$ s, and $t_3 = 12{,}000$ s for the N, R, and S tests are presented in Figures 17, 18 and 19, where the initial profile at $t = 0$ is plotted to indicate the degree of the profile change at the given time. The degree of agreement for each test is explained separately because the revetment and sill have different effects on the beach profile evolution. The measured accretional profiles at time t_1 and t_2 in the N test (Figure 17)

appeared similar to a recovering beach profile after artificial erosion associated with the initial profile creation. CSHORE predicted only minor onshore sand transport near the shoreline. During major wave overtopping from time t_2 to t_3, the berm erosion was predicted better but the eroded berm profile was not reproduced well.

For the R test (Figure 18), the revetment was located in the zone of x = 18.12 – 18.52 m. The measured beach profile changes in front of the revetment at time t_1 and t_2 were accretional and similar to those of the N test but the computed profile changes were slightly erosional. It should be noted that the initial revetment slope was adjusted to match the measured revetment slope at t_2. Erosion of the berm crest caused by wave overtopping from t_2 and t_3 was predicted but the predicted erosion was insufficient because of the assumption of no stone damage and settlement. CSHORE predicted no sand deposition on the filter inside the revetment but the measured average sand height was about 0.3 cm at the end of the R test. No sand deposition implies net offshore sand transport at the revetment toe and net onshore sand transport at the landward end of the revetment.

For the S test (Figure 19), the sill was located in the zone of x = 16.16 – 16.64 m and the adjusted initial sill profile was the sill profile measured at t_1. CSHORE did not predict the formation and growth of a step feature in the zone of x = 17 – 18 m. Slight erosion occurred at the toe of the sill but CSHORE predicted toe accretion. Nevertheless, CSHORE reproduced little profile change at t_1, minor berm erosion at t_2, and major berm erosion at t_3 reasonably. CSHORE predicted sand deposition on the seaward part of the filter and the average sand height of about 0.3 cm in comparison with the measured average height of 0.8 cm.

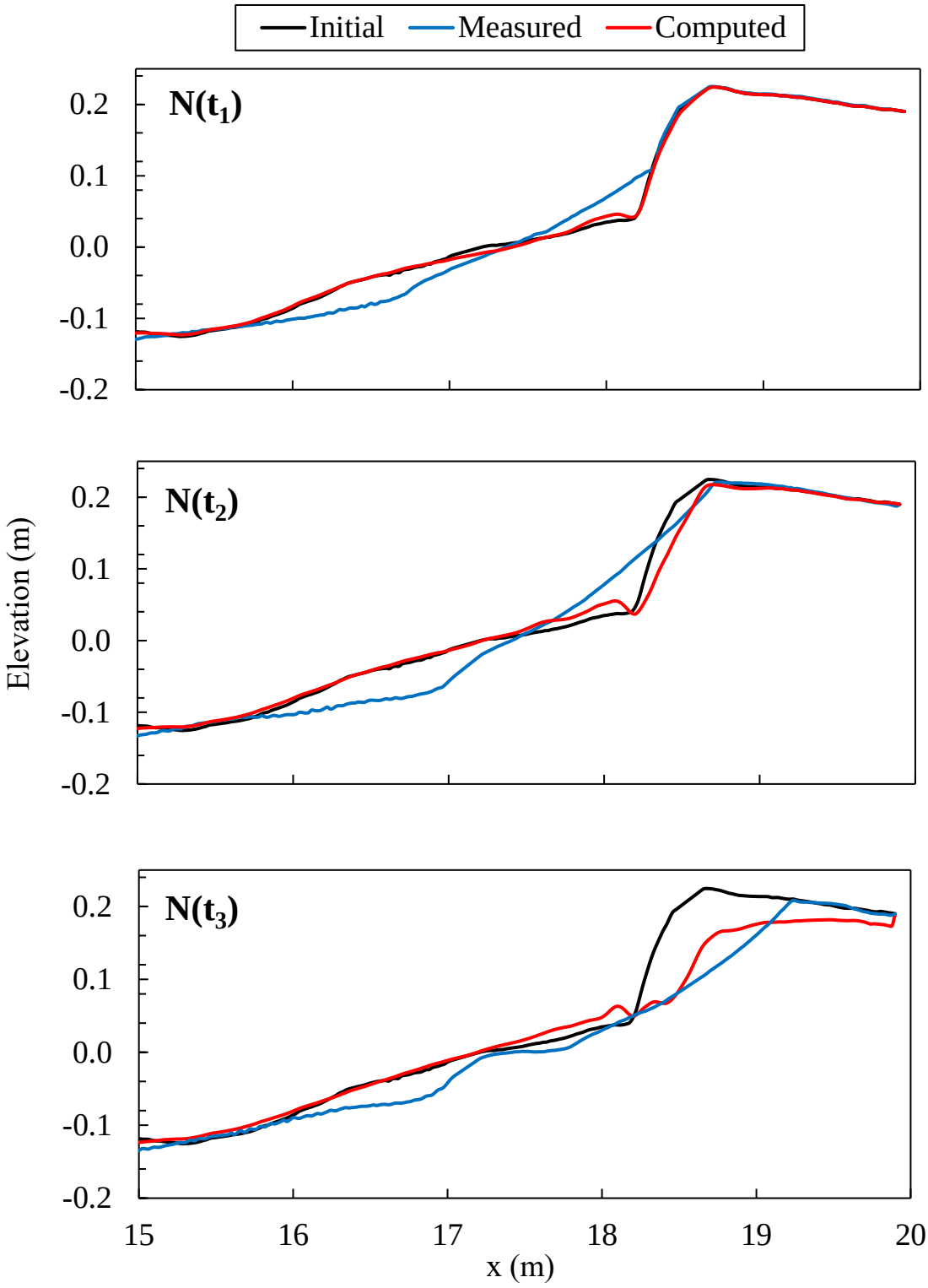

Figure 17: Computed and measured profiles at time t_1 = 4,000 s, t_2 = 8,000 s, and t_3 = 12,000 s for Test N.

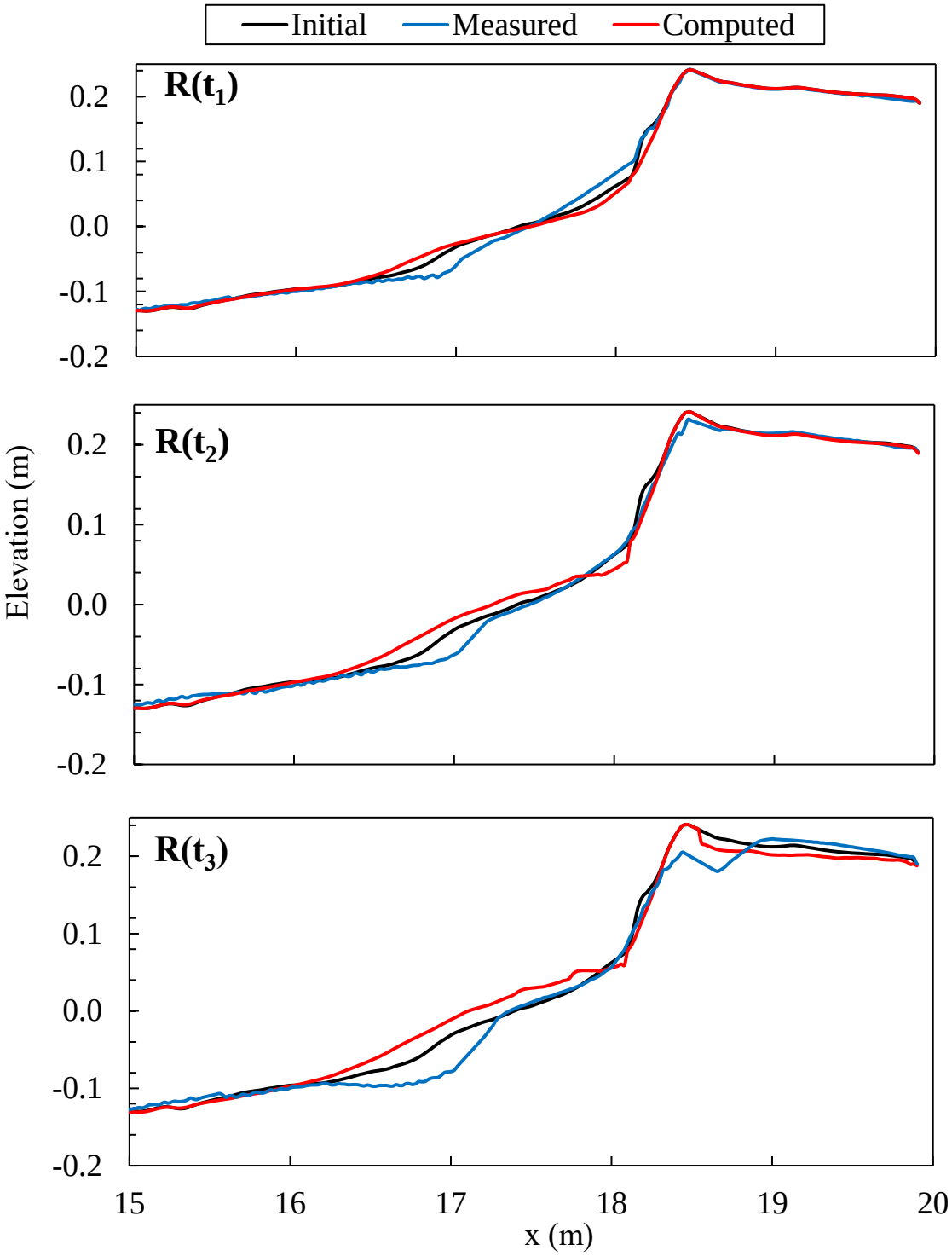

Figure 18: Computed and measured profiles at time t_1 = 4,000 s, t_2 = 8,000 s, and t_3 = 12,000 s for Test R.

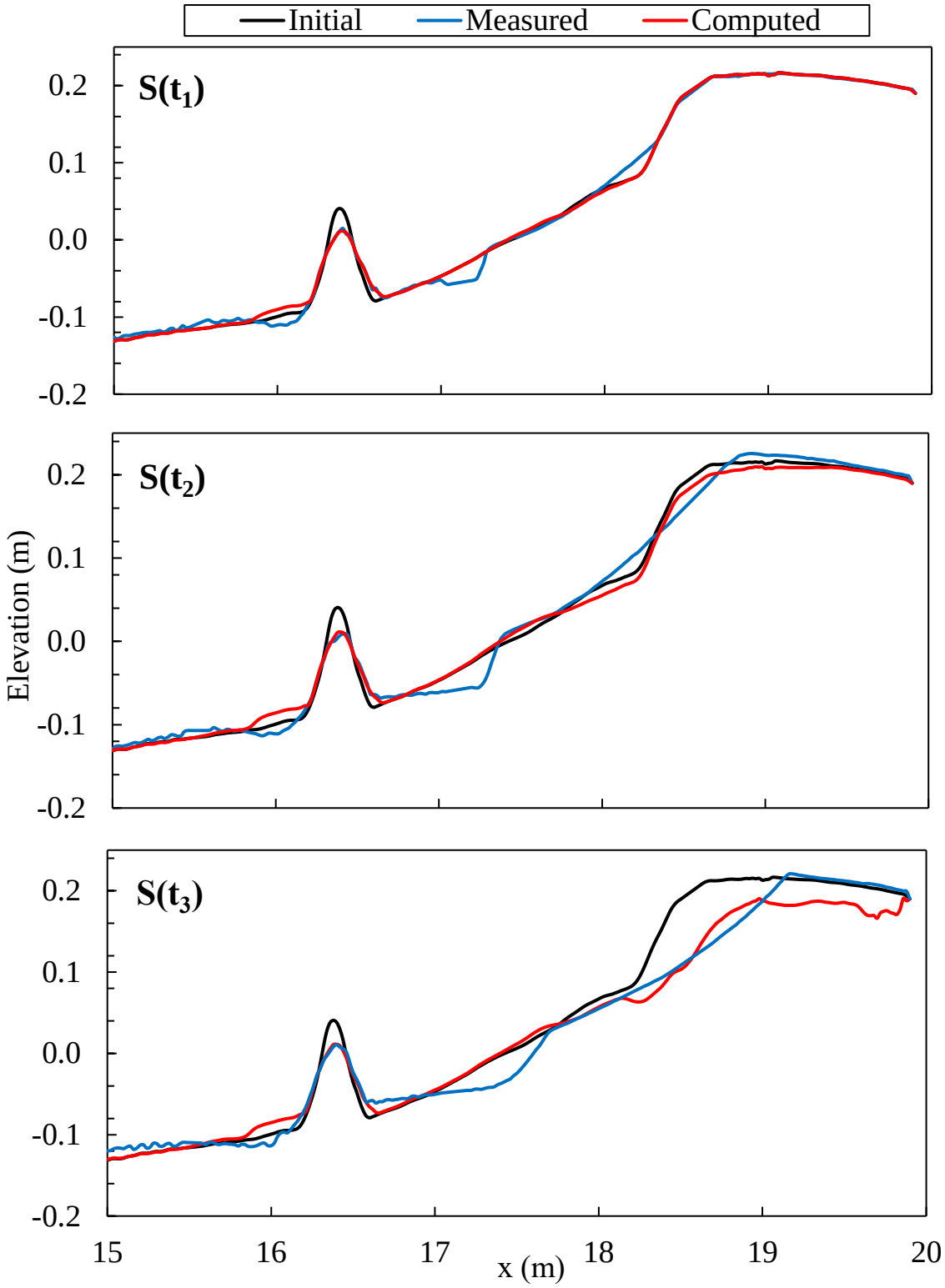

Figure 19: Computed and measured profiles at time t_1 = 4,000 s, t_2 = 8,000 s, and t_3 = 12,000 s for Test S.

No method exists to predict the settlement of a structure built on a sand bottom. Sand transport processes under the filter cannot be predicted at present. The option of no filter added to the upgraded CSHORE is used to estimate the upper limit of the structure settlement. This option allows erosion below the stone structure and deposition inside the porous structure by computing the temporal and cross-shore variation of the sand surface elevation z_p inside the structure. The filter option formulated by Kobayashi and Kim (2017) assumed the lower limit of z_p as the initial filter elevation which was fixed. This restriction was removed in the no filter option. The sand surface elevation z_p decreases for sand erosion and increases for sand deposition. No sand was present on the filter at the start of the R and S tests. Sand erosion implies erosion of sand below the stone structure.

Figure 20 shows the computed cross-shore variation of z_p at time t_3 = 12,000 s in the zone of the structure for the R and S tests. The measured filter elevations at time t = 0 and t_3 in Figure 12 are added in Figure 20 where the initial elevation of z_p was the same as the initial filter elevation. For the R test, the final z_p at t_3 was lower than the initial z_p at t = 0, corresponding to sand erosion and lowering the revetment stone bottom. The stone layer thickness was assumed to be invariant and the structure surface lowering was the same as the structure bottom lowering. The difference between the final filter elevation and the final profile of z_p may be regarded as the settlement reduction provided by the filter. The revetment settlement could be of the order of 0.1-m in the absence of the filter for the R test perhaps because the revetment was built in the zone of large erosion in the N test. For the S test, no filter settlement occurred and the computed final z_p was above the filter near the edges of the sill because of computed sand deposition of about 1-cm. The settlement reduction provided by the filter was relatively small perhaps because the sill was built

in the zone of smaller erosion in the N test.

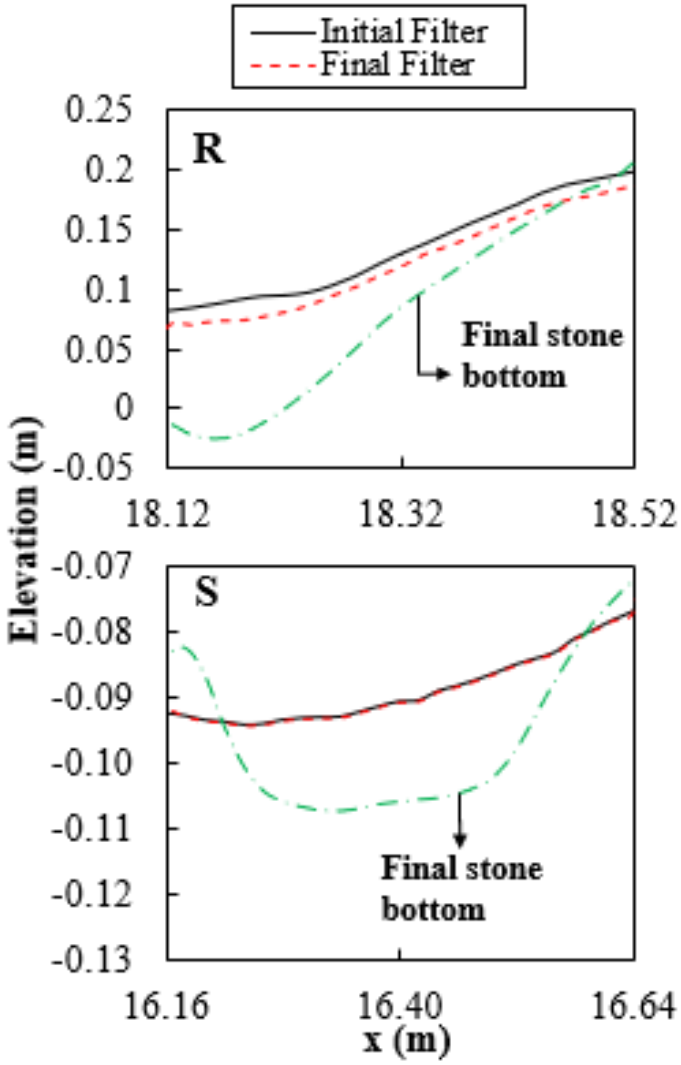

Figure 20: Computed settlement of stone bottom with no filter in comparison with measured filter elevations at start and end of Tests R and S

Chapter 5

CONCLUSIONS

A laboratory experiment consisting of 3 tests was conducted in a wave flume to compare sand beach profile evolution and wave overtopping of a sand berm for the cases of no structure, a stone revetment protecting the steep sand berm, and a stone sill reducing wave action on the berm. The same stones were used to construct the revetment and sill. The revetment reduced onshore sand transport on the sand beach in front of the revetment but was effective in protecting the sand berm and reducing wave overtopping. The settlement of the revetment placed on a filter occurred and the revetment crest was damaged during major wave overtopping. The sill reduced the beach profile change but was not very effective in reducing wave overtopping and berm erosion when the sill crest was submerged sufficiently. Piled stones on the narrow sill crest were displaced. The lowered and wider crest was more stable. The settlement of the sill placed on the filter did not occur perhaps because the sill was placed on the beach in the zone of minor erosion in the test of no structure. For the three tests, the revetment was more effective in reducing shore erosion and wave overtopping. The sill provided a zone of reduced wave action when the sill crest was above or near the still water level.

The cross-shore numerical model CSHORE was upgraded for its application to the sill test where the emerged sill crest became submerged during the test. The wave transformation was predicted within errors of 20 % except for the persistent underprediction of the local wave height immediately landward of the sill. The wave overtopping and overwash rates were predicted within errors of 100 % but the small rates were predicted only within a factor of 10. The reduced beach profile changes in the presence of the revetment and sill were reproduced but CSHORE could not

produce sufficient onshore sand transport near the shoreline. The upgraded CSHORE included an option of no filter to predict the settlement of the stone structure caused by sand erosion below the structure and to estimate the settlement reduction provided by the filter in the revetment and sill tests. This option will need to be verified by future tests. Finally, CSHORE should be compared with field data in order to demonstrate its utility for field applications.

REFERENCES

Ahrens, J. 1989. "Stability of reef breakwaters." J. Waterway, Port, Coastal, Ocean Eng., 10.1061/(ASCE)0733-950X(1989)115:2(221), 221-234.

Faraci, C., Scandura, P., and Foti, E. 2014. "Bottom profile evolution of a perched nourished beach." J. Waterway, Port, Coastal, Ocean Eng., 10.1061/(ASCE)WW.1943-5460.0000253, 04014021.

Figlus, J., Kobayashi, N., and Gralher, C. 2012. "Onshore migration of emerged ridge and ponded runnel." J. Waterway, Port, Coastal, Ocean Eng., 10.1061/(ASCE)WW.1943-5460.0000139, 331-338.

Figlus, J., Kobayashi, N., Gralher, C., and Iranzo, V. 2011. "Wave overtopping and overwash of dunes." J. Waterway, Port, Coastal, Ocean Eng., 10.1061/(ASCE)WW.1943-5460.0000060, 26-33.

Garcia, R., and Kobayashi, N. 2015. "Trunk and head damage on a low-crested breakwater." J. Waterway, Port, Coastal, Ocean Eng., 10.1061/(ASCE)WW.1943-5460.0000276, 04014037.

Hardaway, C.S., Milligan, D.A., and Duhring, K. 2010. "Living shoreline design guidelines for shore protection in Virginia's estuarine environments." Special Report No. 421, Virginia Institute of Marine Science, College of William & Mary, Gloucester Point, Virginia.

Kim, H.D., Kobayashi, N., and Cardenas, X. C. 2016. "Comparison of rock seawall and dune for storm damage reduction." Proc. 35th Int. Conf. on Coastal Engineering, ASCE, Reston, VA,1-13.

Kobayashi, N. 2016. "Coastal sediment transport modeling for engineering applications." J. Waterway, Port, Coastal, Ocean Eng., 10.1061/(ASCE)WW.1943-5460.0000347, 03116001.

Kobayashi, N., Cox, D.T., and Wurjanto, A. 1990. “Irregular wave reflection and runup on rough impermeable slopes.” J. Waterway, Port, Coastal, Ocean Eng., 116 (6), 708-726.

Kobayashi, N., Farhadzadeh, A., and Melby, J.A. 2010. “Wave overtopping and damage progression of stone armor layer.” J. Waterway, Port, Coastal, Ocean Eng., 136 (5), 257-265.

Kobayashi, N., and Kim, H.D. 2017. “Rock seawall in the swash zone to reduce wave overtopping and overwash of a sand beach.” J. Waterway, Port, Coastal, Ocean Eng., 10.1061/(ASCE)WW.1943-5460.0000416, 04017033.

Kobayashi, N., Meigs, L.E., Ota, T., and Melby, J.A. 2007. “Irregular breaking wave transmission over submerged porous breakwaters. J. Waterway, Port, Coastal, Ocean Eng., 10.1061/(ASCE)0733-950X(2007)133:2(104), 104-116.

Kobayashi, N., Pietropaolo, J., and Melby, J. 2013. “Deformation of reef breakwaters and wave transmission.” J. Waterway, Port, Coastal, Ocean Eng., 10.1061/(ASCE)WW.1943-5460.0000180, 336-340.

Kobayashi, N., Zhu, T., and Mallavarapu, S. 2018. “Equilibrium beach profile with net cross-shore sand transport.” J. Waterway, Port, Coastal, Ocean Eng., 10.1061/(ASCE)WW.1943-5460.0000469, 04018016.

Melby, J., and Kobayashi, N. 1998. “Progression and variability of damage on rubble mound breakwaters.” J. Waterway, Port, Coastal, Ocean Eng., 10.1061/(ASCE)0733-950X(1998)124:6(286), 286-294.

Musumeci, R.E., Cavallaro, L., and Foti, E. 2012. “Performance of perched beach nourishments.” Proc. 33rd Int. Conf. on Coastal Engineering, ASCE, Reston, VA, 1-13.

Needelman, B.A., Crooks, S., Shumway, C.A., Titus, J.G., Takacs, R., and Hawkes, J.E. 2012. "Restore-adopt-mitigate: Responding to climate change through coastal habitat restoration." Restore America's Estuaries, Washington, D.C.

USACE (US Army Corps of Engineers). 2002. Coastal engineering manual. Washington, DC: USACE.